JAERI-M
93-138

ASSESSMENT OF TRAC-PF1/MOD1 AND TRAC-PF1/MOD2 CODES FOR THERMAL-HYDRAULIC BEHAVIOR IN PRESSURE VESSEL DURING REFLOOD IN SCTF TEST WITH AN INCLINED RADIAL POWER DISTRIBUTION

July 1993

Akira OHNUKI, Hajime AKIMOTO and Yoshio MURAO

日本原子力研究所
Japan Atomic Energy Research Institute

JAERI-Mレポートは，日本原子力研究所が不定期に公刊している研究報告書です。
入手の問合わせは，日本原子力研究所技術情報部情報資料課（〒319-11茨城県那珂郡東海村）あて，お申しこしください。なお，このほかに財団法人原子力弘済会資料センター（〒319-11 茨城県那珂郡東海村日本原子力研究所内）で複写による実費頒布をおこなっております。

JAERI-M reports are issued irregularly.
Inquiries about availability of the reports should be addressed to Information Division Department of Technical Information, Japan Atomic Energy Research Institute, Tokai-mura, Naka-gun, Ibaraki-ken 319-11, Japan.

編集兼発行　日本原子力研究所
印　　刷　いばらき印刷㈱

JAERI-M 93-138

Assessment of TRAC-PF1/MOD1 and TRAC-PF1/MOD2 Codes for Thermal-hydraulic Behavior in Pressure Vessel during Reflood in SCTF Test with an Inclined Radial Power Distribution

Akira OHNUKI, Hajime AKIMOTO and Yoshio MURAO

Department of Reactor Engineering
Tokai Research Establishment
Japan Atomic Energy Research Institute
Tokai-mura, Naka-gun, Ibaraki-ken

(Received June 8, 1993)

Post test calculations for the Slab Core Test Facility (SCTF) Test S3-15 which had an inclined radial power distribution were performed to assess the TRAC-PF1/MOD1 (MOD1) and the TRAC-PF1/MOD2 (MOD2) codes for the thermal-hydraulic behaviors including two-dimensional behaviors in pressure vessel during reflood phase of a PWR-LOCA. In this report, it was mainly assessed whether the predictability of the MOD2 code was improved compared to that of the MOD1 code or not. In the MOD2 code, the core thermal-hydraulic model during reflood and the numerical scheme for pressure vessel have been changed from those in the MOD1 code.

The predictions by the MOD2 code was improved qualitatively for the hydraulic behaviors in pressure vessel although the characteristics of water accumulation in the upper plenum was different from measured results. The quantitative difference between the MOD2 code predictions and the data was large for the void fraction in the lower half of core. The predictability of the MOD2 code for the core heat transfer was degraded compared to that of the MOD1 code.

Time step size in the MOD2 calculation was larger than that in the MOD1 calculation due to the change of numerical scheme for VESSEL component and the calculational speed in the MOD2 calculation was almost 1.5 times faster than that in the MOD1 calculation.

Keywords: Reactor Safety, Heat Transfer, Void Fraction, Two-phase Flow, Reflood, Film Boiling, Numerical Simulation, TRAC Code

傾斜出力分布を有するＳＣＴＦ試験の圧力容器内における再冠水時熱水力学的挙動に対するＴＲＡＣ－ＰＦ１／ＭＯＤ１及びＴＲＡＣ－ＰＦ１／ＭＯＤ２コードの予測性能評価

日本原子力研究所東海研究所原子炉工学部
大貫　晃・秋本　肇・村尾　良夫

（1993年６月８日受理）

ＰＷＲ－ＬＯＣＡ時再冠水過程での，圧力容器内における二次元挙動を含む熱水力挙動に対するＴＲＡＣ－ＰＦ１／ＭＯＤ１（ＭＯＤ１）及びＴＲＡＣ－ＰＦ１／ＭＯＤ２（ＭＯＤ２）コードの予測性能を評価するために，炉心半径方向に傾斜した出力分布をもつ平板炉心試験装置（ＳＣＴＦ）試験Ｓ３－１５に対する試験後解析を行った。本報告では，ＭＯＤ２コードの予測性能がＭＯＤ１コードのものに比べ改善されたか否かを主に評価した。ＭＯＤ２コードはＭＯＤ１コードに比べ，再冠水時の炉心内熱水力モデル及び圧力容器内の数値解法が変更されている。

上部プレナム内の蓄水特性は測定結果と異なったものの，圧力容器内の水力挙動に対するＭＯＤ２コードの予測性能はＭＯＤ１コードのものより定性的には改善された。定量的には，炉心中央より下におけるボイド率に対する予測誤差が大きかった。また炉心熱伝達に対するＭＯＤ２コードの予測性能はＭＯＤ１コードのものより劣化した。

ＭＯＤ２コードによる計算でのタイムステップサイズはＶＥＳＳＥＬコンポーネントでの数値解法の変更によりＭＯＤ１コードによるものより大きく，ＭＯＤ２コードの計算速度はＭＯＤ１コードの約1.5倍となった。

東海研究所：〒319-11　茨城県那珂郡東海村白方字白根2-4

Contents

目　　次

List of Tables

List of Figures

1. Introduction

The International Thermal-Hydraulic Code Assessment and Application Program (ICAP) was conducted by several countries and coordinated by the United States Nuclear Regulatory Commission (USNRC).[1] The purpose of ICAP is to make qualitative and quantitative statement regarding the accuracy of the current thermal-hydraulic computer programs developed under the auspices of the USNRC.

Japan's contributions to ICAP include the assessment of TRAC-PWR[2], TRAC-BWR[3] and RELAP5[4] codes. The assessment matrix is shown in Table 1. The assessment calculations were conducted by Japan Atomic Energy Research Institute (JAERI) and Japanese industrial groups.

In this report, the predictive capability of TRAC-PF1/MOD1 (Version 12.5)[2] and TRAC-PF1/MOD2 (Version 5.3)[5] codes is presented for the thermal-hydraulic behaviors including two-dimensional behaviors in pressure vessel during reflood phase of a postulated Large Break Loss-of-Coolant Accident (LBLOCA) in a PWR. Ohnuki et al. reported with data of the Slab Core Test Facility (SCTF)[6] test with a steep radial power profile that the TRAC-PF1/MOD1 (MOD1) code predicts transients of clad surface temperature well including the radial distribution caused by different bundle power but the MOD1 code predicts poor agreement for the void fraction in the core.[7] In the TRAC-PF1/MOD2 (MOD2) code, a new core thermal hydraulic model for the reflood is incorporated and the numerical scheme for VESSEL component is changed to save computational time, the component which has a capability to calculate three-dimensional thermal-hydraulics of two-phase flow. In this report, the predictive capability of the MOD1 code is further assessed using data of the SCTF test S3-15[8] which has an inclined radial power distribution and we also assess the predictability of the new reflood model in the MOD2 code by comparing with the data and the results with the MOD1 code.

This report is organized as follows: Chapter 2 describes the test facility and test conditions and Chapter 3 describes the TRAC input model used to simulate the test. In Chapter 4, results from the simulations are presented and discussed. Summary and recommendations are presented in Chapter 5.

2. Facility and Test Description

2.1 Test Facility

The SCTF was designed to properly simulate the two-dimensional core heat transfer and hydraulic behaviors during refill-reflood phase. The pressure vessel is of slab geometry as shown in Fig. 2.1.1. Full scale radial and axial section of a reference PWR is provided as a simulated core with single bundle depth. The reference reactor of the SCTF Core－Ⅲ test is the Siemens type reactor in Germany which is a four loop 1300 MWe PWR. The simulated core consists of 8 bundles arranged in a row. On the other hand, simplified primary coolant loops are provided. Bird's-eye view of pressure vessel and the coolant loop is shown in Fig. 2.1.2. The scaling of flow area and fluid volume of each component is in accordance with the core flow area scaling. The principal dimensions of the facility is shown in Table 2.1.1, and the comparison of dimensions between the SCTF and the referred PWR is shown in Table 2.1.2.

Each bundle has 236 electrically heated rods and 20 non-heated rods. The arrangement of rod bundles is shown in Fig. 2.1.3. The dimensions of the heater rods are based on a 15x15 type fuel bundle and the heated length and the outer diameter of each heater rod are 3.613 m and 10.7 mm, respectively. The dimension, configuration and axial power distribution of each heater rod are shown in Figs. 2.1.4, 2.1.5 and 2.1.6. The axial peaking factor is 1.4. The heater rods and non-heated rods are fixed at the top of the core allowing the rods to move downward when the thermal expansion occurs. For better simulation for flow resistance in the lower plenum, the simulated rods do not penetrate through the bottom plate of the lower plenum.

The design of upper plenum internals is based on that of the referred reactor. The arrangement of the internals is shown in Fig. 2.1.7.

Mode detailed information on the SCTF Core－Ⅲ is available in reference (8).

2.2 Test Conditions and Procedure

Emergency core cooling (ECC) water was injected into the lower plenum in the test examined in this report, Test S3-15. Since the bottom of downcomer in the test was opened, the test was performed under so-called gravity reflood condition. In the test S3-15, the radial power distribution was inclined, i.e. the normalized radial power factor in bundles 1, 2, 3, 4, 5, 6, 7 and 8 were 1.36, 1.2, 1.1, 1.0, 0.9, 0.86, 0.81 and 0.76, respectively. Major measured test conditions are listed in Tables 2.2.1.

The test procedure for the test was as follows. After setting the initial conditions (pressure and saturation condition, etc.), core heating was initiated. When four cladding temperatures exceeded 1038K, the accumulator (Acc) injection into the lower plenum was initiated. The initial saturation water level in the lower plenum was about 0.519m below the bottom of heated part. The maximum cladding temperature at the reflood initiation was intended to be 1108K. At the initiation of Acc injection, the core power decay simulation started from the value at 40s after shutdown of an actual reactor. The decay curve was based on the "1.02 x (ANS standard + actinides)". Chronology of major events in the test is shown in Table 2.2.2.

3. Code and Model Description

3.1 Input Schematics

The TRAC input in this report modeled the pressure vessel, ECC injection piping and a hot leg in SCTF. Intact and broken cold legs and steam/water separator were not modeled because of the following reasons:

(1) Main assessment subject is the two−dimensional thermal−hydraulic behaviors in the pressure vessel in this report and

(2) Since the SCTF has the steam/water separator instead of steam generators to measure carry−over flow rate accurately, the effect of the feed back from the exit of the hot leg is negligible small on the core behaviors in the SCTF.

The pressure vessel was represented by VESSEL component as shown in Fig. 3.1.1. The bottom of downcomer was blocked to supply a specified flow rate at the core inlet accurately. The noding consists of 18 axial levels, 11 radial sections and 1 azimuthal section. Levels 4 through 9 and radial sections 1 through 8 represent the heated core.

The ECC injection piping and the hot leg were modeled by PIPE components as shown in Fig. 3.1.2. Mass flow rate and fluid temperature of ECC water was supplied by FILL component. The boundary condition at the exit of the hot leg was supplied by BREAK component.

The ECC injection piping is connected to the cell of level 1 and radial section 9 of VESSEL component as shown in Fig. 3.1.1. And the hot leg is connected to the cell of level 16 and radial section 9 of VESSEL component as also shown in Fig. 3.1.1.

The TRAC input data for the MOD1 and the MOD2 codes were intended to be the same for the geometry and the boundary conditions. However, the following modifications

The test procedure for the test was as follows. After setting the initial conditions (pressure and saturation condition, etc.), core heating was initiated. When four cladding temperatures exceeded 1038K, the accumulator (Acc) injection into the lower plenum was initiated. The initial saturation water level in the lower plenum was about 0.519m below the bottom of heated part. The maximum cladding temperature at the reflood initiation was intended to be 1108K. At the initiation of Acc injection, the core power decay simulation started from the value at 40s after shutdown of an actual reactor. The decay curve was based on the "1.02 x (ANS standard + actinides)". Chronology of major events in the test is shown in Table 2.2.2.

3. Code and Model Description

3.1 Input Schematics

The TRAC input in this report modeled the pressure vessel, ECC injection piping and a hot leg in SCTF. Intact and broken cold legs and steam/water separator were not modeled because of the following reasons:

(1) Main assessment subject is the two-dimensional thermal-hydraulic behaviors in the pressure vessel in this report and

(2) Since the SCTF has the steam/water separator instead of steam generators to measure carry-over flow rate accurately, the effect of the feed back from the exit of the hot leg is negligible small on the core behaviors in the SCTF.

The pressure vessel was represented by VESSEL component as shown in Fig. 3.1.1. The bottom of downcomer was blocked to supply a specified flow rate at the core inlet accurately. The noding consists of 18 axial levels, 11 radial sections and 1 azimuthal section. Levels 4 through 9 and radial sections 1 through 8 represent the heated core.

The ECC injection piping and the hot leg were modeled by PIPE components as shown in Fig. 3.1.2. Mass flow rate and fluid temperature of ECC water was supplied by FILL component. The boundary condition at the exit of the hot leg was supplied by BREAK component.

The ECC injection piping is connected to the cell of level 1 and radial section 9 of VESSEL component as shown in Fig. 3.1.1. And the hot leg is connected to the cell of level 16 and radial section 9 of VESSEL component as also shown in Fig. 3.1.1.

The TRAC input data for the MOD1 and the MOD2 codes were intended to be the same for the geometry and the boundary conditions. However, the following modifications

were made for the VESSEL component in the MOD2 code input:

(1) Friction factors multiplied by hydraulic diameters were adopted to meet the requirements of MOD2 code input[5] and

(2) The elevations of grid spacers and the fraction of non−heated wall were added to apply the new reflood model developed by Los Alamos National Laboratory[5].

The model for the countercurrent flow limitation (CCFL) was not used in this MOD2 code calculation.

3.2 Initial and Boundary Conditions

The initial and time−dependent boundary conditions were determined based on the measured data. The mass flow rate and the fluid temperature of ECC water which was supplied by FILL component were estimated by a system mass balance and an energy balance. The pressure at the exit of hot leg which was supplied by BREAK component was represented by the pressure measured at the steam/water separator in the test. The conditions for FILL, supplied core power and BREAK are shown in Figs.3.2.1 through 3.2.3. These values are plotted against the time after core power on.

The conditions for FILL are shown in Fig. 3.2.1 and the upper figure of Fig. 3.2.2. The input values for TRAC calculations are found to agree well with the data. The condition for BREAK is compared in the lower figure of Fig. 3.2.2. The initial and time−dependent values agree well with the data. The total supplied power for bundles 1, 4 and 8 is compared in Fig. 3.2.3. Radial distribution of supplied power and the shape of decay curve are the same as those in the test.

4. Results and Discussion

4.1 Hydraulic Behavior in Pressure Vessel except Core

In this section, the assessment results are discussed on the pressure in the pressure vessel, the core inlet fluid temperature, the mass flow rate at the exit of the core, the mass flow rate at the exit of the hot leg and the amount of water accumulation in the upper plenum.

Figure 4.1.1 shows the comparison of the pressure in the upper plenum, in the core and in the lower plenum. The whole transients are almost predicted qualitatively and quantitatively by both codes. However, the MOD2 code slightly underestimates in the lower plenum after about 200 sec. The difference was caused by the underestimation for

were made for the VESSEL component in the MOD2 code input:

(1) Friction factors multiplied by hydraulic diameters were adopted to meet the requirements of MOD2 code input[5] and

(2) The elevations of grid spacers and the fraction of non−heated wall were added to apply the new reflood model developed by Los Alamos National Laboratory[5].

The model for the countercurrent flow limitation (CCFL) was not used in this MOD2 code calculation.

3.2 Initial and Boundary Conditions

The initial and time−dependent boundary conditions were determined based on the measured data. The mass flow rate and the fluid temperature of ECC water which was supplied by FILL component were estimated by a system mass balance and an energy balance. The pressure at the exit of hot leg which was supplied by BREAK component was represented by the pressure measured at the steam/water separator in the test. The conditions for FILL, supplied core power and BREAK are shown in Figs.3.2.1 through 3.2.3. These values are plotted against the time after core power on.

The conditions for FILL are shown in Fig. 3.2.1 and the upper figure of Fig. 3.2.2. The input values for TRAC calculations are found to agree well with the data. The condition for BREAK is compared in the lower figure of Fig. 3.2.2. The initial and time−dependent values agree well with the data. The total supplied power for bundles 1, 4 and 8 is compared in Fig. 3.2.3. Radial distribution of supplied power and the shape of decay curve are the same as those in the test.

4. Results and Discussion

4.1 Hydraulic Behavior in Pressure Vessel except Core

In this section, the assessment results are discussed on the pressure in the pressure vessel, the core inlet fluid temperature, the mass flow rate at the exit of the core, the mass flow rate at the exit of the hot leg and the amount of water accumulation in the upper plenum.

Figure 4.1.1 shows the comparison of the pressure in the upper plenum, in the core and in the lower plenum. The whole transients are almost predicted qualitatively and quantitatively by both codes. However, the MOD2 code slightly underestimates in the lower plenum after about 200 sec. The difference was caused by the underestimation for

core differential pressure as will be presented in Figs. 4.2.1 through 4.2.3.

Figures 4.1.2 and 4.1.3 show the comparison of the core inlet fluid temperature just below bundles 1, 4 and 8. The fluid temperature predicted by the MOD2 code is higher than the data during whole transients except in the early period. On the other hand, the agreement between the data and the MOD1 code predictions is better but the radial difference among the three locations is slightly larger than the data. Since the liquid down−flow rate in lower power bundles into the lower plenum was higher in the MOD2 code calculation than that in the MOD1 code calculation as will be shown in Figs.4.2.10(1) and 4.2.10(2), the higher temperature is considered to be caused by the liquid circulation between the core and the lower plenum.

Figure 4.1.4 shows the comparison of the integrated carry−over liquid mass at the top of core and at the exit of hot leg. For the liquid carry−over at the top of core, the MOD2 code almost predicts the data but the MOD1 code underestimates the data. For the liquid carry−over at the exit of hot leg, the MOD2 code almost predicts the data until about 400 sec but after about 400 sec the MOD2 code overestimates the carry−over rate. On the other hand, the MOD1 code predicts almost no carry−over until about 650 sec. These results indicate that the MOD2 code predictions for the carry−over behavior are improved compared to the MOD1 code predictions.

Figure 4.1.5 shows the comparison of steam mass flow rate at the exit of hot leg. Both code predictions almost agree with the data although some differences are recognized until about 200 sec. The MOD1 code underestimates the steam mass flow rate until about 200 sec. The MOD2 code overestimates in an initial period. These differences on the steam mass flow rate until about 200 sec are considered to be caused by the different characteristics for the liquid accumulation in the core because in each period the MOD1 code predicts almost no liquid accumulation in the upper half of core and the MOD2 code overestimates the liquid accumulation in the central region of core as will be shown in Figs. 4.2.4 through 4.2.6.

Figure 4.1.6 shows the comparison of differential pressures in the upper plenum above bundles 1, 4 and 8 and the comparison of radial difference of the differential pressure as (Differential pressure above bundle 8 − that above bundle 1). The MOD1 code almost predicts the differential pressure above each bundle but the radial difference is not predicted qualitatively and quantitatively. The MOD1 code prediction for the radial difference is flatter than the data. On the other hand, the MOD2 code predictions for the differential pressure above each bundle show an irregular increase or decrease and have

a tendency to be higher than the data. For the radial difference, the MOD2 code almost predicts the data qualitatively and quantitatively. These results indicate that the prediction for the two-dimensional hydraulic behaviors in upper plenum is improved in the MOD2 code calculation but the prediction for the transient of differential pressure above each bundle is degraded.

4.2 Hydraulic Behavior in Core

Figures 4.2.1 through 4.2.3 show the comparisons of differential pressures in the upper half, the lower half and the full height of core in bundles 2, 4 and 8, respectively. For the full height of core, the MOD1 code overestimates the differential pressure and the MOD2 code underestimates the differential pressure. The overestimation in the MOD1 code calculation is caused by the overestimation in the lower half of core until about 500 sec and after the time the overestimation in the upper half of core. The underestimation in the MOD2 code calculation is mainly caused by the underestimation in the lower half of core. The MOD2 code almost predicts the differential pressure in the upper half of core until about 500 sec. These tendencies for the differential pressure prediction are also recognized for the predictions on the void fraction in the core discussed below.

Figures 4.2.4 through 4.2.6 show the comparison of sectional void fraction at three axial sections in bundles 2, 4 and 8, respectively. The MOD1 code tends to predict no water accumulation in the early period and to overestimate the water accumulation in the middle and top regions of core in the later period. The characteristic of this peculiar axial distribution is the same as the results in Ref. (6) and the tendency was reported to be caused by the interface sharpener model in the MOD1 code. On the other hand, the MOD2 code predictions give similar water accumulation behavior compared to the data in the middle and the top regions of core although the MOD2 code overestimates the void fraction in the later period. For the bottom region of core, the MOD2 code overestimates the void fraction with a spiky oscillation.

Figures 4.2.7 and 4.2.8 show the comparison of the radial difference of void fraction among bundles 2, 4 and 8 at the middle region of core. The SCTF data indicate that the void fraction in bundles 2 and 4 (higher power bundles) is lower than that in bundle 8 (lower power bundle) until about the time that quench fronts reach at the bottom of each section and after the time the void fraction in bundles 2 and 4 is higher than that in bundle 8. The MOD1 code do not predict the tendency observed in the data. On the other hand, the MOD2 code predicts the lower void fraction in the lower power bundle

during almost whole transients. The tendency of the MOD2 code predictions corresponds to that in the data after the time that the quench front reaches at the bottom of the section but the tendency of the data until the time is not predicted.

Figures 4.2.9(1), 4.2.9(2), 4.2.10(1) and 4.2.10(2) show the comparison between the MOD1 code and the MOD2 code predictions for the two-dimensional steam and liquid mass flow rate distribution in the core at a specified time. These figures also include the location of quench fronts calculated by each code at each time. The following remarks are recognized from these figures,

(1) Steam mass flow rate gradually increases from around the quench front to the top of the core, and the radial distribution of axial steam mass flow rate is flatter in the MOD1 code calculation than that in the MOD2 code calculation due to the higher cross flow rate in the core,

(2) For the liquid flow rate distribution in the MOD1 code calculation, the systematic circulation of liquid flow is not recognized but

(3) In the MOD2 code calculation, the liquid in higher power bundles flows upwards and the liquid in lower power bundles flows downwards. In the lower power bundles, the liquid down-flow from the upper plenum is observed.

4.3 Thermal Behavior in Core

Figures 4.3.1 through 4.3.3 show the comparison of clad surface temperature in bundles 2, 4 and 8, respectively. The MOD1 code almost predicts the shape of transient curve of the temperature and the time of quench. On the other hand, the MOD2 code predicts later quench time at 0.95m and 1.905m elevations in bundles 2 and 4 and shorter quench time at 3.19m elevation although the turnaround temperature in those bundles are predicted well by the MOD2 code. For the bundle 8, the MOD2 code overestimates the heat transfer at 1.905 m and 3.19 m elevations.

Figures 4.3.4 through 4.3.7 show the comparison of the turnaround temperature and quench time along the axial direction in bundles 2, 4 and 8. For the turnaround temperature, the MOD2 code predicts the data in the higher power bundles (Bundles 2 and 4) better than the MOD1 code but underestimates that in the low power bundle (Bundle 8). Both codes overestimate the radial difference of the turnaround temperature. For the quench propagation, the MOD1 code predicts well the data including the radial difference. The MOD2 code underestimates the quench velocity in the higher power bundles and overestimates the area of so-called top quench region. The MOD2 code also

overestimates the radial difference of the quench velocity. The results in this section indicate that the degree of the agreement between the MOD2 code and the data for the core heat transfer is degraded compared to that between the MOD1 code and the data.

4.4 Run Statistics

The calculations in this report were performed with FACOM-M780 computer at JAERI. The integrated time step number and the time step size are compared in Fig. 4.4.1. Summary table for run statistics is listed below:

Code	Transient time (s) RT	Total CPU time (s) CPU	Total time step number ST	CPU/RT	CPU/ST (S)	RT/ST (S)
MOD1	698	24984	72040	35.8	0.347	0.0097
MOD2	748	18000	22350	24.06	0.805	0.0335

The time step size (RT/ST) is larger and the total time step number is reduced in the MOD2 code calculation compared to those in the MOD1 code calculation. These results can be considered to be caused by the change of the numerical scheme in the MOD2 code for VESSEL component as mentioned in Introduction. If the CPU time within one time step is the same between each other, the value of RT/ST in the above list indicates that the calculation with the MOD2 code is expected to be about 3 times faster. However, the new scheme requires more CPU time within one time step as indicated in the item of CPU/ST in the above list. As the result, the MOD2 code gave about 1.5 times faster calculation than the MOD1 code as indicated in the above item of CPU/RT.

5. Summary and Recommendation

TRAC−PF1/MOD1 (Version 12.5) and TRAC−PF1/MOD2 (Version 5.3) simulations have been conducted to assess the predictive capability for the thermal−hydraulic behaviors including two−dimensional behaviors in pressure vessel during reflood phase in a large break LOCA of PWR. The test selected for the assessment was the SCTF Test S3−15 which had an inclined radial power distribution.

The assessment results are summarized as the following:

(1) The MOD1 code predicted transients of clad surface temperature well including radial distribution caused by different bundle power. The MOD2 code predicted later quench time in higher power bundles than the data although the turnaround temperature in the higher power bundles were predicted well. The MOD2 code overestimates the heat transfer in low power bundle.

(2) The axial and radial distributions of core void fraction were not predicted well with the MOD1 code. The interface sharpener model of the MOD1 code gave the curious axial void fraction profile. In the predictions with the MOD2 code, the characteristics of void fraction transients became similar to those in the test but the void fraction in the lower half of core was overestimated.

(3) The MOD1 code underestimated the amount of integrated liquid carry−over mass at the top of core and at the exit of hot leg. The vertical differential pressure in the upper plenum was almost predicted with the MOD1 code but the radial distribution was flatter compared to measured results. The MOD2 code almost predicted the amount of integrated liquid carry−over mass out of core and at the exit of hot leg but predicted an irregular increase or decrease along the transients for the vertical differential pressure in the upper plenum.

(4) Time step size in the MOD2 calculation was larger than that in the MOD1 calculation due to the change of numerical scheme for VESSEL component and the calculational speed in the MOD2 calculation was almost 1.5 times faster than that in the MOD1 calculation.

The results in the above items (1), (2) and (3) indicate that the predictability of the MOD2 code is improved compared to the MOD1 code for the hydraulic behaviors in pressure vessel although the characteristic of vertical differential pressure in the upper plenum is different from the measured results qualitatively. However, the difference of core void fraction between the predictions and the data is still large quantitatively

especially in the lower half of core. The predictability of the MOD2 code for the core heat transfer is degraded.

Since the heat transfer model is closely related to the local void fraction in the TRAC code, it is recommended to improve further the hydraulic models related to the quantitative difference for the void fraction as the first approach. After the elimination of the difference, the core heat transfer model should be improved. The measured data used in this study was obtained under the two−dimensional reflooding condition and local flow conditions were not measured. Therefore, further reflood model improvement should be performed by using data obtained under a fixed conditions, such as the data in FLECHT[9] and those in Small Scale Reflood Test at JAERI[10].

Acknowledgments

The authors wish to express their thanks to the members of the SCTF analysis group, Drs. H. Adachi, T. Iwamura and Y. Abe for valuable discussions. The authors appreciate Mr. M. Enomoto for his assistance on performing the conversion of TRAC−PF1/MOD2 code from CRAY version to FACOM version.

especially in the lower half of core. The predictability of the MOD2 code for the core heat transfer is degraded.

Since the heat transfer model is closely related to the local void fraction in the TRAC code, it is recommended to improve further the hydraulic models related to the quantitative difference for the void fraction as the first approach. After the elimination of the difference, the core heat transfer model should be improved. The measured data used in this study was obtained under the two−dimensional reflooding condition and local flow conditions were not measured. Therefore, further reflood model improvement should be performed by using data obtained under a fixed conditions, such as the data in FLECHT[9] and those in Small Scale Reflood Test at JAERI[10].

Acknowledgments

The authors wish to express their thanks to the members of the SCTF analysis group, Drs. H. Adachi, T. Iwamura and Y. Abe for valuable discussions. The authors appreciate Mr. M. Enomoto for his assistance on performing the conversion of TRAC−PF1/MOD2 code from CRAY version to FACOM version.

References

(1) USNRC: Guidelines and Procedures for the International Code Assessment and Applications Program, NUREG-1271 (1987).

(2) Liles, D.R., et al.: TRAC-PF1/MOD1 ; An Advanced Best-Estimate Computer Program for Pressurized Water Reactor Thermal-Hydraulic Analysis, NUREG/CR-3858 (1986).

(3) Taylor, D.D., et al.: TRAC-BD1/MOD1 ; An Advanced Best-Estimate Computer Program for Boiling Water Reactor Transient Analysis, NUREG/CR-3633 (1984).

(4) Ransom, V., et al.: RELAP5/MOD2 Code Manual, NUREG/CR-4312 (1985).

(5) Schnurr, N.M., et al.: TRAC-PF1/MOD2 Code Manual, NUREG/CR-5673 LA-12031-M (1992).

(6) Adachi, H., et al.: Design of Slab Core Test Facility (SCTF) in Large Scale Reflood Test Program, Part 1 : Core-1, JAERI-M 83-080 (1983).

(7) Ohnuki, A. et al.: Assessment of TRAC-PF1/MOD1 Code for Thermal-hydraulic Behavior including Two-dimensional behavior in Pressure Vessel during Reflood in SCTF, To be published as JAERI-M report.

(8) Iwamura, T. et al.: Evaluation Report on SCTF Core-Ⅲ Tests S3-14, S3-15 and S3-16 (Effects of Radial Power Profile Shape on Two-dimensional Thermal-hydraulic Behavior in Core), JAERI-M 88-060 (1988).

(9) Cadek, F.F., et al.: PWR FLECHT (Full length emergency cooling heat transfer) final report, WCAP-7665 (1971).

(10) Ohnuki, A., et al.: Effect of Liquid Flow Rate on Film Boiling Heat Transfer during Reflood in Rod Bundle, J. Nucl. Sci. Technol., 27(6) 535-546 (1990).

Table 1 ICAP assessment matrix - Japan

	LOCA type	TRAC-P				RELAP5				TRAC-B				
		88	89	90	91	88	89	90	91	88	89	90	91	
CCTF	PWR LB	9	1				5				5			Reflood
SCTF	PWR LB	3	5	3			1				1			Reflood
ROSA-Ⅱ	PWR LB								2					Blowdown
ROSA-Ⅲ	BWR LB/SB										1	1		Blowdown
ROSA-Ⅳ	PWR SB	1	1(0)			1	0(1)							
TBL	BWR LB/SB										1	1		Blowdown
Total		13	7(6)	3		1	6(7)		2		8	2		42

Table 2.1.1 Principal dimensions of SCTF core-III

1. Core Dimension			
(1)	Quantity of Bundle	8 Bundles	
(2)	Bundle Array	1 x 8	
(3)	Bundle Pitch	230 mm	
(4)	Rod Array in a Bundle	16 x 16	
(5)	Rod Pitch in a Bundle	14.3 mm	
(6)	Quantity of Heater Rod in a Bundle	236 rods	
(7)	Quantity of Non−Heater Rod in a Bundle	20 rods	
(8)	Total Quantity of Heater Rods	236x8=1,888 rods	
(9)	Total Quantity of Non−Heated Rods	20x8=160 rods	
(10)	Effective Heated Length of Heater Rod	3613	mm
(11)	Diameter of Heater Rod	10.7	mm
(12)	Diameter of Non−Heated Rod	13.8	mm
2. Flow Area & Fluid Volume			
(1)	Core Flow Area	0.25	m^2
(2)	Core Fluid Volume	0.903	m^3
(3)	Baffle Region Flow Area (isolated)	(0.096)	m^2
(4)	Baffle Region Fluid Volume (nominal)	0.355	m^3
(5)	Cross−Sectional Area of Core Additional Fluid Volumes including Gap between Core Barrel and Pressure Vessel Wall and Various Penetration Holes	0.07 0.10	m^2 m^2
(6)	Downcomer Flow Area	0.158	m^2
(7)	Upper Annulus Flow Area	0.158	m^2
(8)	Upper Plenum Horizontal Flow Area (max.)	0.541	m^2
(9)	Upper Plenum Vertical flow Area	0.525	m^2
(10)	Upper Plenum Fluid Volume	1.156	m^3
(11)	Upper Head Fluid Volume	0.86	m^3
(12)	Lower Plenum Fluid Volume (excluding below downcomer)	1.302	m^2
(13)	Steam Generator Inlet Plenum Simulator Flow Area	0.626	m^2
(14)	Steam Generator Inlet Plenum Simulator Fluid Volume	0.931	m^3

Table 2.1.1 (Continued)

(15)	Steam Water Separator Fluid Volume	5.3	m^3
(16)	Flow Area at the Top Plate of Steam Generator Inlet Plenum Simulator	0.195	m^2
(17)	Hot Leg Flow Area	0.0826	m^2
(18)	Intact Cold Leg Flow Area (Diameter=297.9 mm) Inverted U-tube with 0.0314 m^2 cross-sectional area (Diameter = 200 mm) and 10 m height from the top of steam generator inlet plenum simulator can be added as an option.	0.0697	m^2
(19)	Broken Cold Leg Flow Area (Diameter=151.0 mm)	0.0179	m^2
(20)	Containment Tank-I Fluid Volume	30	m^3
(21)	Containment Tank-II Fluid Volume	50	m^3
3.	Elevation & Height		
(1)	Top Surface of Upper Core Support Plate (UCSP)	0	mm
(2)	Bottom Surface of UCSP	− 40	mm
(3)	Top of the Effective Heated Length of Heater Rod	− 440	mm
(4)	Bottom of the Effective Heated Length of Heater Rod	− 4053	mm
(5)	Bottom of the Skirt in the Lower Plenum	− 5270	mm
(6)	Bottom of Intact Cold Leg	+ 724	mm
(7)	Bottom of Hot Leg	+ 1050	mm
(8)	Top of Upper Plenum	+ 2200	mm
(9)	Bottom of Steam Generator Inlet Plenum Simulator	+ 1933	mm
(10)	Centerline of Loop Seal Bottom	− 2281	mm
(11)	Bottom Surface of End Box	− 263	mm
(12)	Top of Upper Annulus of Downcomer	+ 2234	mm
(13)	Height of Steam Generator Inlet Plenum Simulator	1438	mm
(14)	Height of Loop Seal	3140	mm
(15)	Inner Height of Hot Leg Pipe	737	mm
(16)	Bottom of Lower Plenum	− 5772	mm
(17)	Top of Upper Head	+ 2887	mm

Table 2.1.2 Comparison of dimensions between the SCTF core-III and the 1300 MWe Siemens PWR

	SCTF	PWR	Ratio (SCTF/PWR)
Quantity of Bundle	8	193	1/24.1
Number of Heater Rod	1888	45548	1/24.1
Number of Rods	2048	49408	1/24.1
Effective Length of Heater Rod (mm)	3613	3900	1/1.08
Rod Pitch (mm)	14.30	14.27	1/0.998
Diameter of Heater Rod (mm)	10.70	10.73	1/1.00
Diameter of Unheated Rod (mm)	13.80	13.80	1/1.00
Flow Area between Core Walls (m^2)	0.250	5.508	1/22.0
Cross-Section Area of Core Additional Fluid Volume (m^3)	0.07~0.10	−	−
Fluid Volume of Core Enveloped by Wall Plates	0.903	21.48	1/23.8
Fluid Volume of Lower Plenum Excluding below Downcomer (m^3)	1.305	28.87	1/22.1
Fluid Volume of Upper Head (m^3)	0.86	18.41	1/21.4
Baffle Region Flow Area (m^2)	(0.096)	1.073	(1/10.7~1/15.3)*
Upper Plenum Fluid Volume (m^3)	1.14	38.77	1/34.0
Downcomer Flow Area (m^2)	0.158	4.636	1/29.3
UCSP Thickness (m^3)	0.04	0.04	1/1.00
Steam Generator Inlet Plenum Simulator Volume (m^2)	0.931	4.99x4	1/21.4
Height of Steam Generator Inlet Plenum Simulator (m)	1.595	1.33	1.0.834
Flow Area at the Top Plate of Steam Generator Inlet Plenum Simulator (m^2)	0.19	1.233x4	1/26.0
Major Axis Length of Hot Leg Cross Section (mm)	737	750	1/1.02
Flow Area of Hot Leg (m^2) (4 Loops)	0.0826	0.4418x4	1/21.4
Flow Area of Intact Loop (m^2) (3 Loops)	0.0696	0.4418x3	1/19.0

Table 2.1.2 (Continued)

Flow Area of Broken Cold Leg (m^2)	0.0179	0.4418	1/24.7

* SCTF Core-III Core Baffle Region Is Isolated but the Core Additional Fluid Volumes Act Like Core Baffle during Transient.

Table 2.2.1 Test conditions for Test S3-15

System pressure	0.2 MPa
Initial total power	7.12 MW
Decay curve	1.02 (ANs + Act.) from 40 s after shutdown
Radial power	inclined*
Initial peak cladding temperature	1108 K (specified) 1151 K (measured)
ECC water injection mode	Gravity feed, lower plenum injection
ECC water flow rate Acc (maximum) LPCI (after 100 s)	37 kg/s 3.75 kg/s
ECC water flow rate Acc LPCI (after 28 s)	353 K 393 K

* Power ratio	1.36	:	1.2	:	1.1	:	1.0	:	0.9	:	0.86	:	0.81	:	0.76
Bundle No.	1		2		3		4		5		6		7		8

Table 2.2.2 Chronology of major events for Test S3-15

	Time after core power "ON"	Time after reflood initiation
Core power "ON"	0 s	−122 s
ECC injection initiation	114	−8
Core power decay initiation	122	0
Reflood initiation	122	0
Maximum core temperature (1183 K)	140	18
Maximum pressure at the top of containment tank-II (0.227 MPa)	146	24
Maximum pressure at the center of core (0.258 MPa)	155	33
Whole core quenched	574.5	452.5

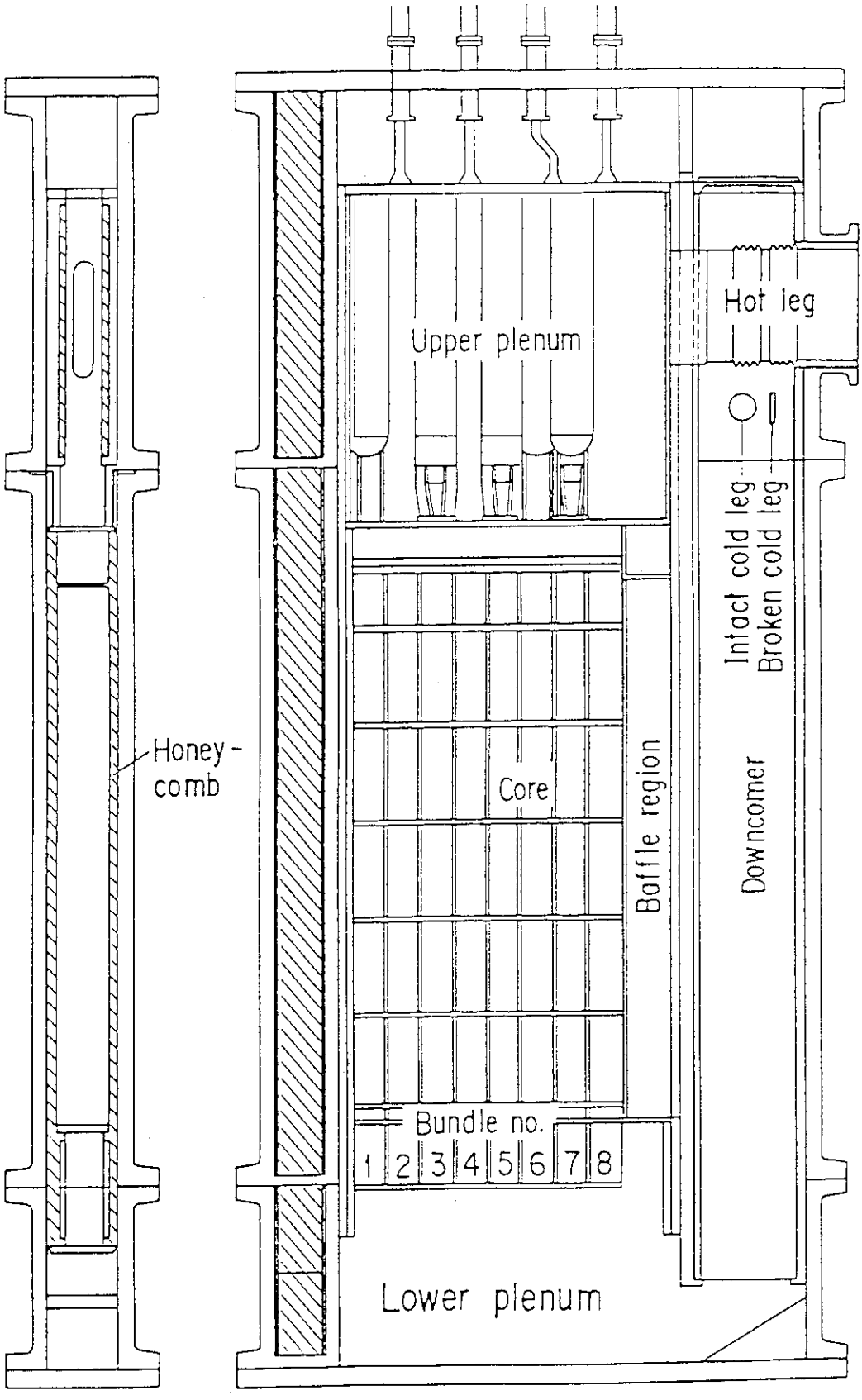

Fig. 2.1.1 Vertical cross sections of pressure vessel

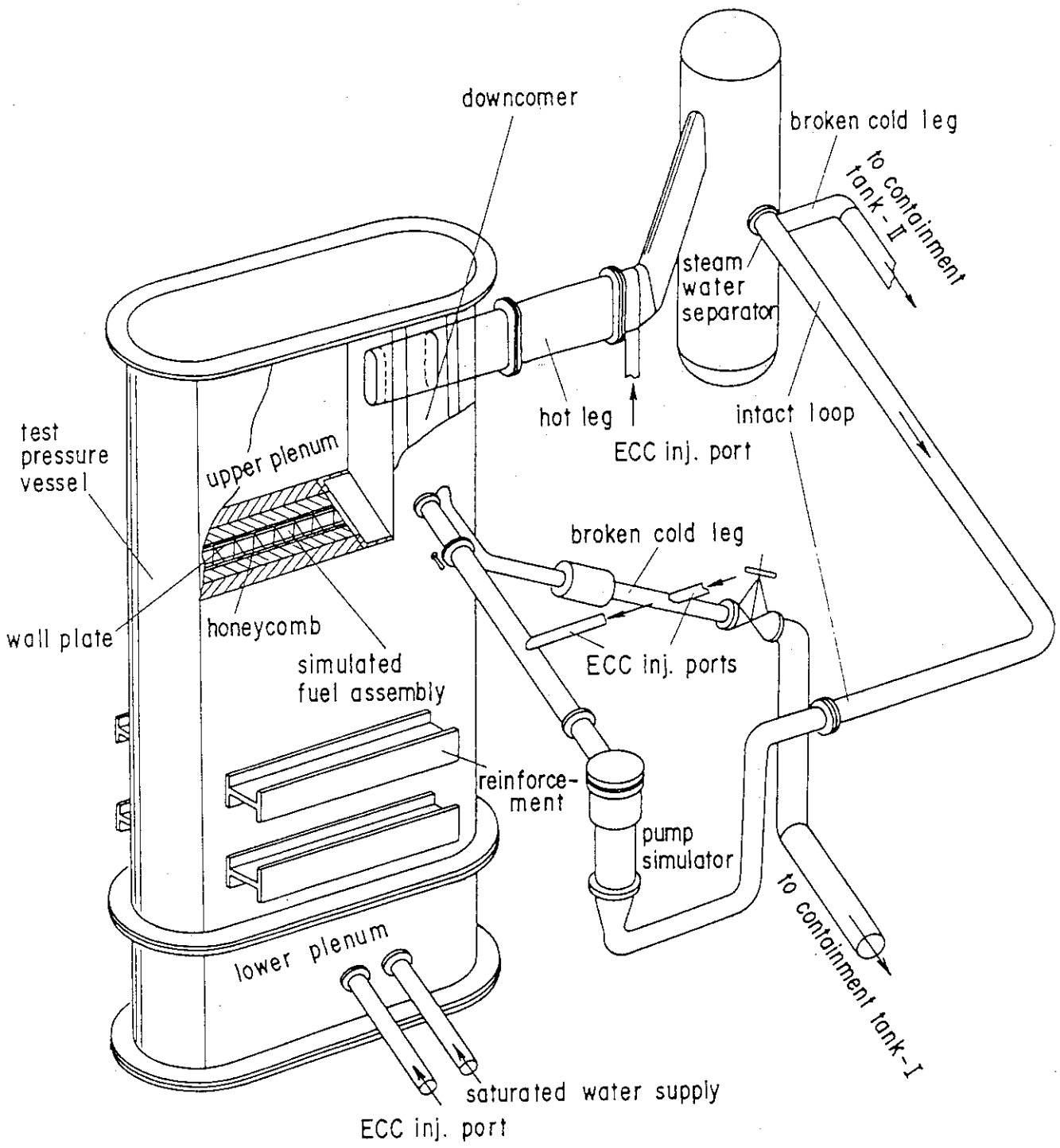

Fig. 2.1.2 Bird's-eye view of SCTF

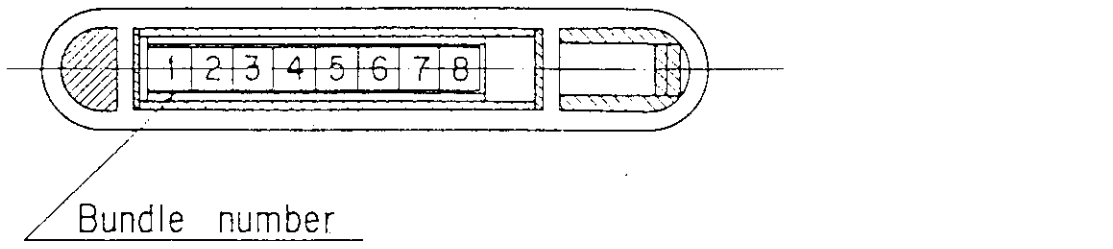

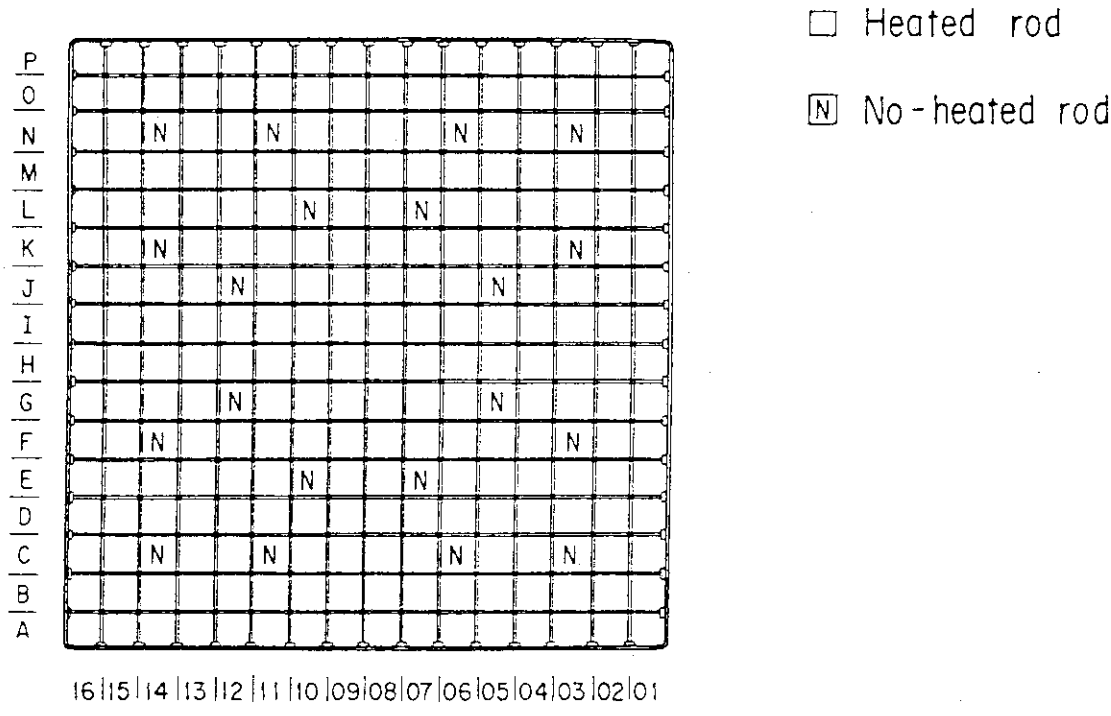

Fig. 2.1.3 Arrangement of rod bundles

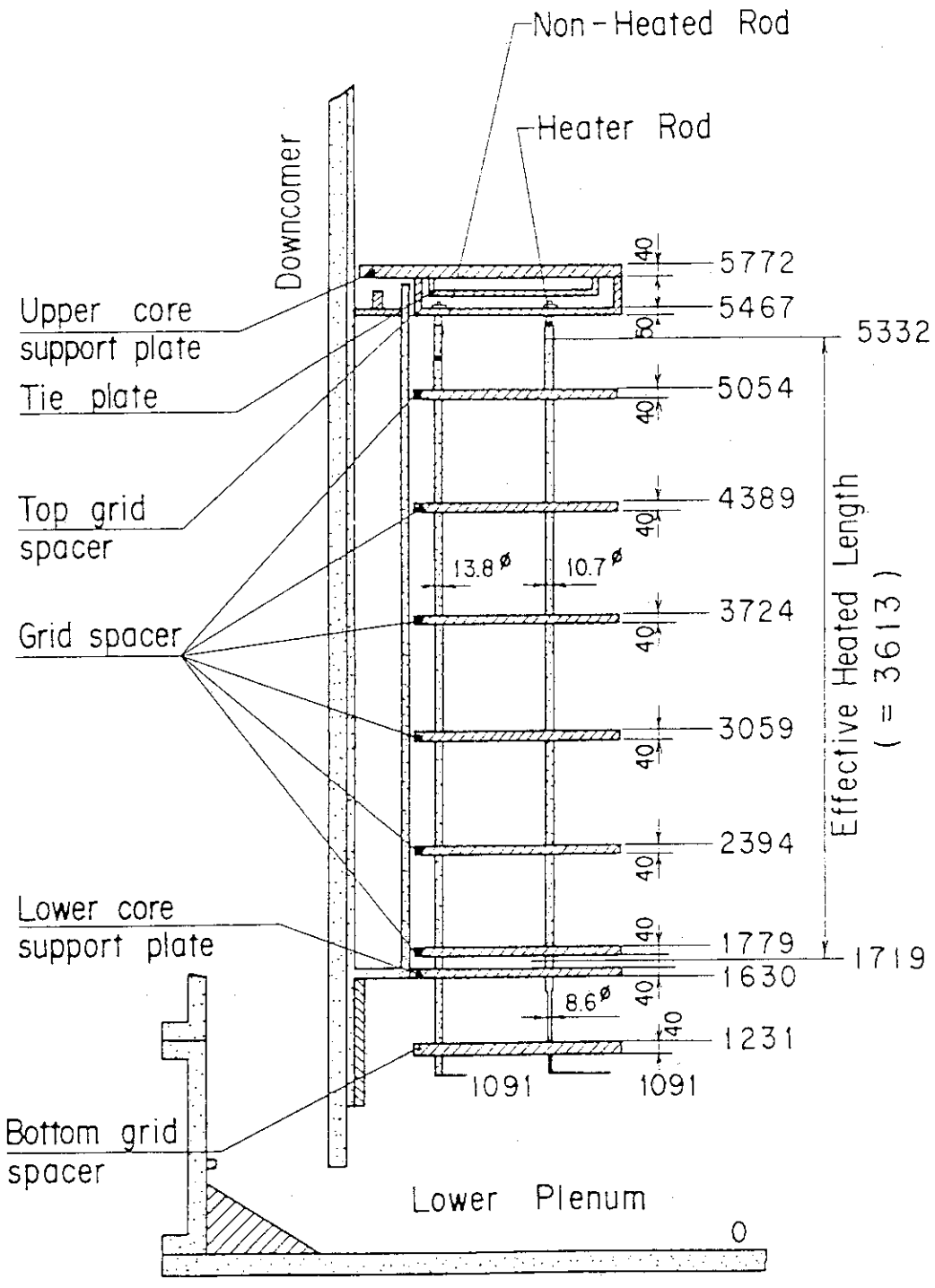

Fig. 2.1.4 Relative elevation and dimension of the core in SCTF

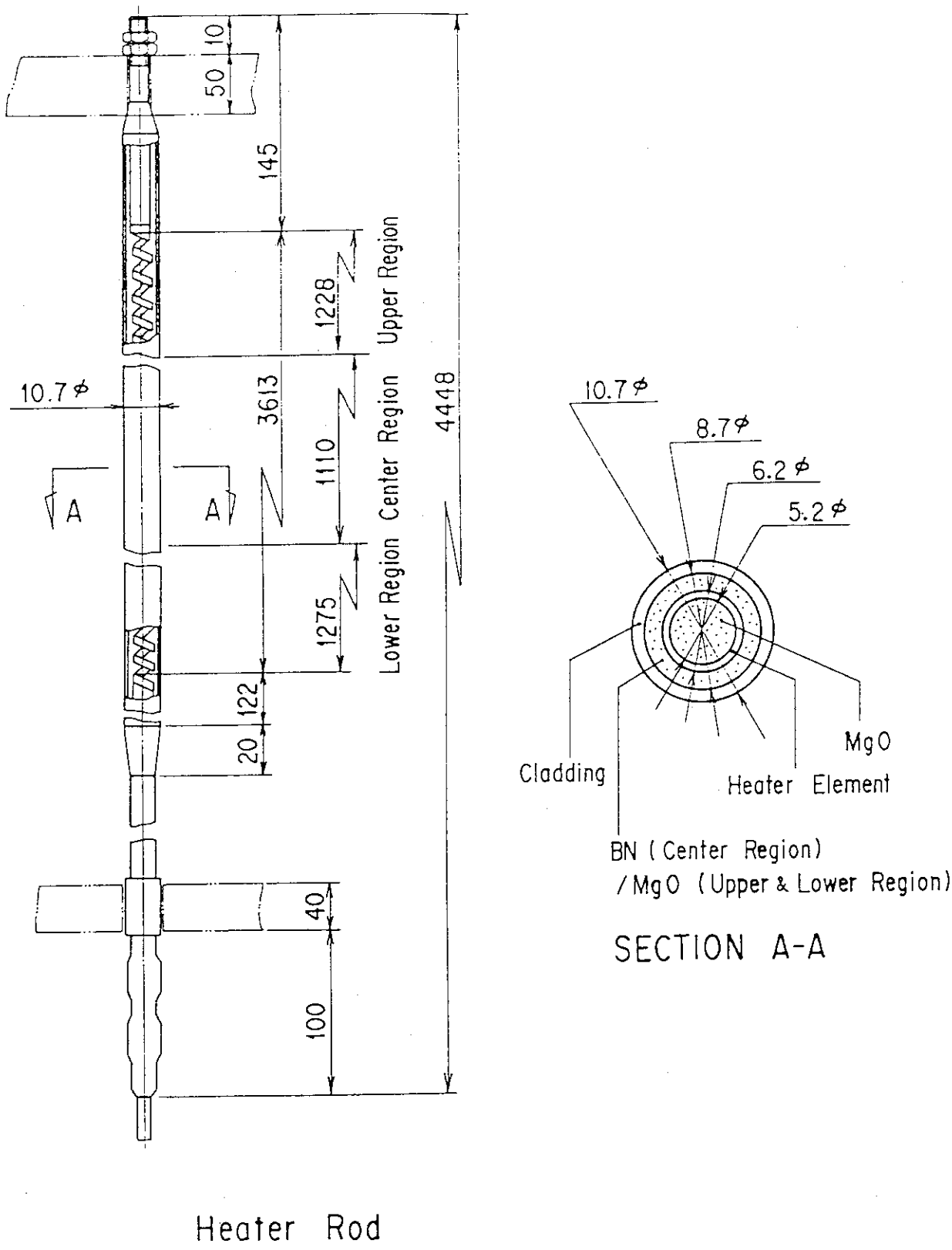

Fig. 2.1.5 Dimension and configuration of heater rods

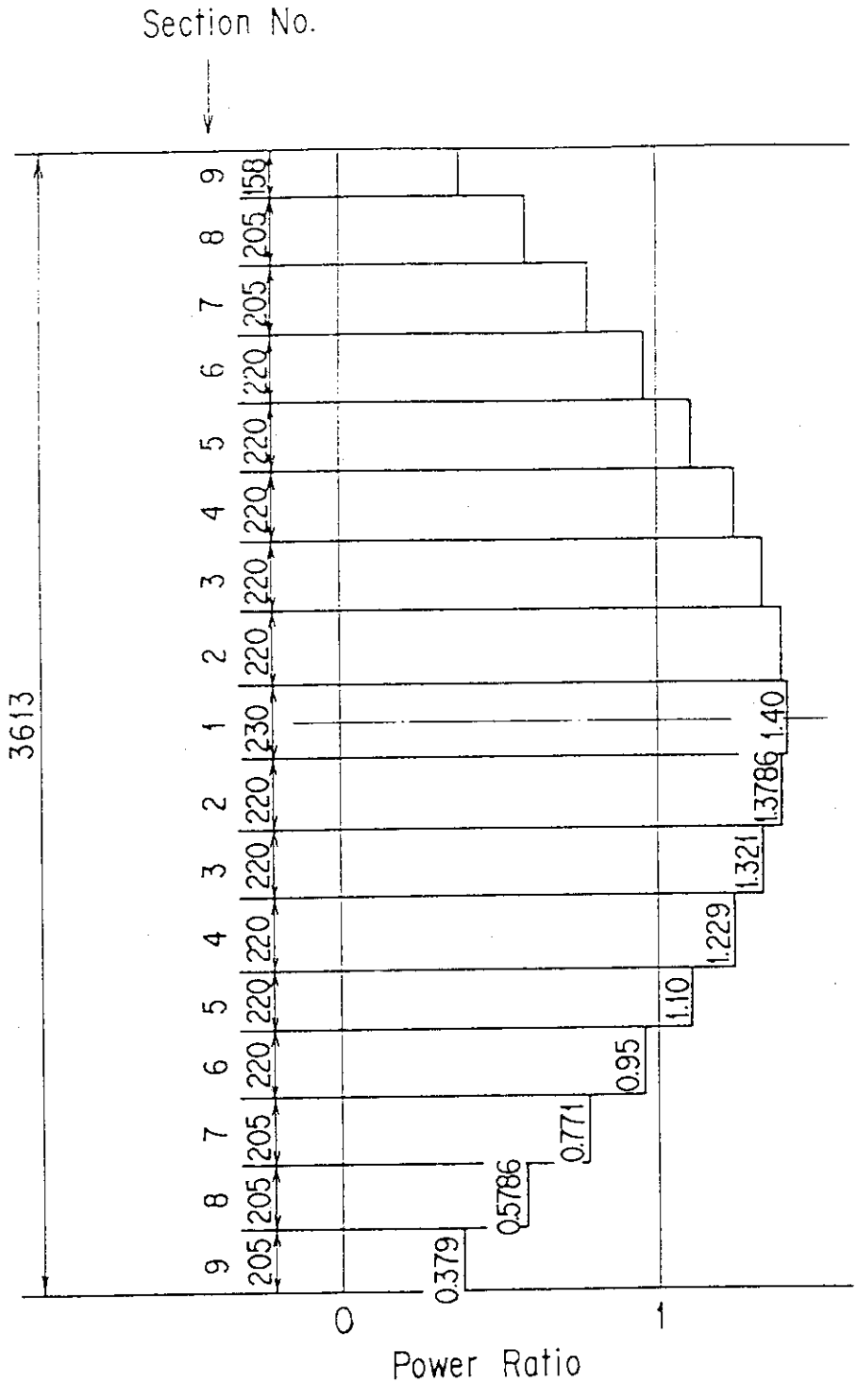

Fig. 2.1.6 Axial power distribution of heater rods

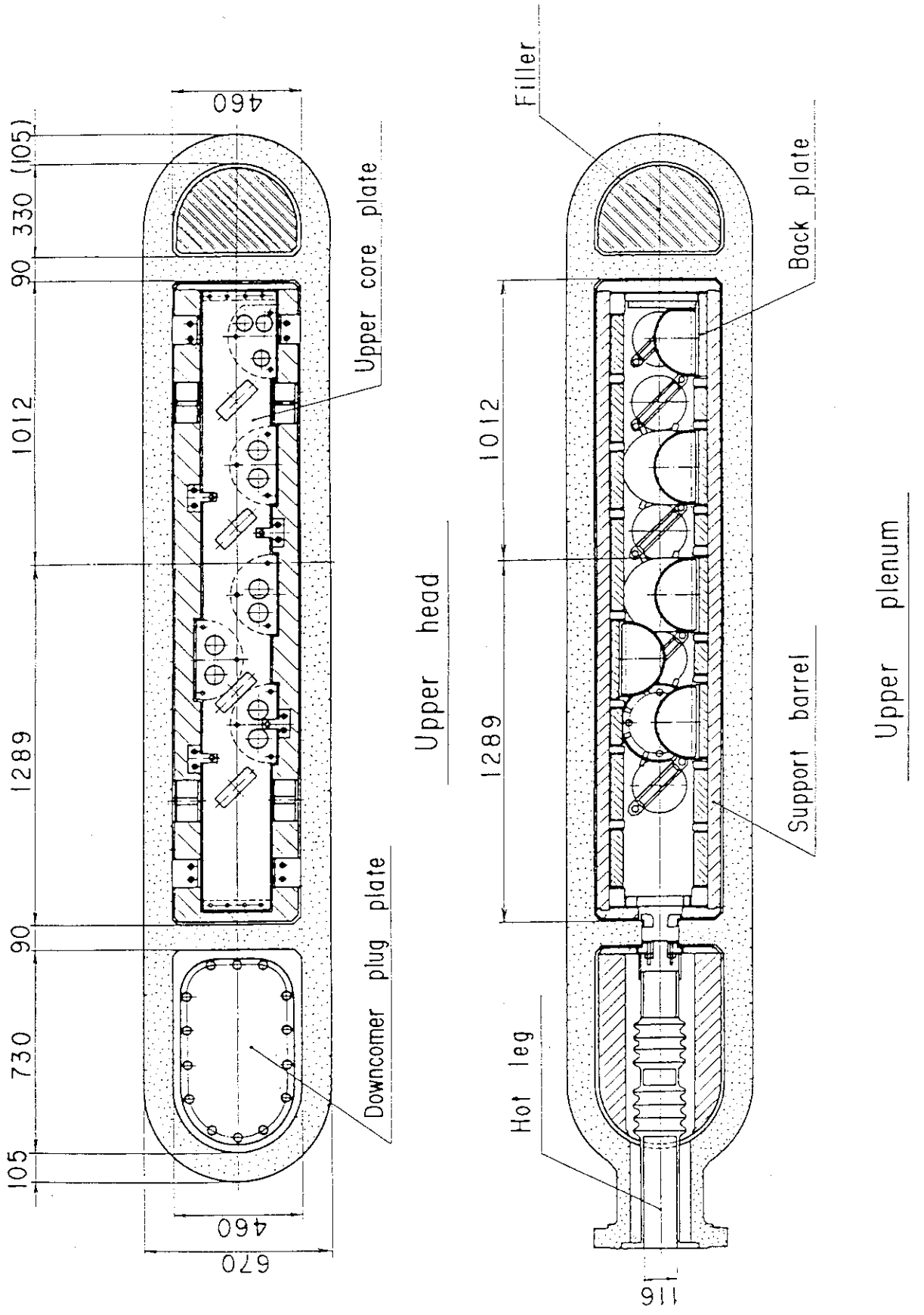

Fig. 2.1.7 Horizontal cross sections in upper head and in upper plenum

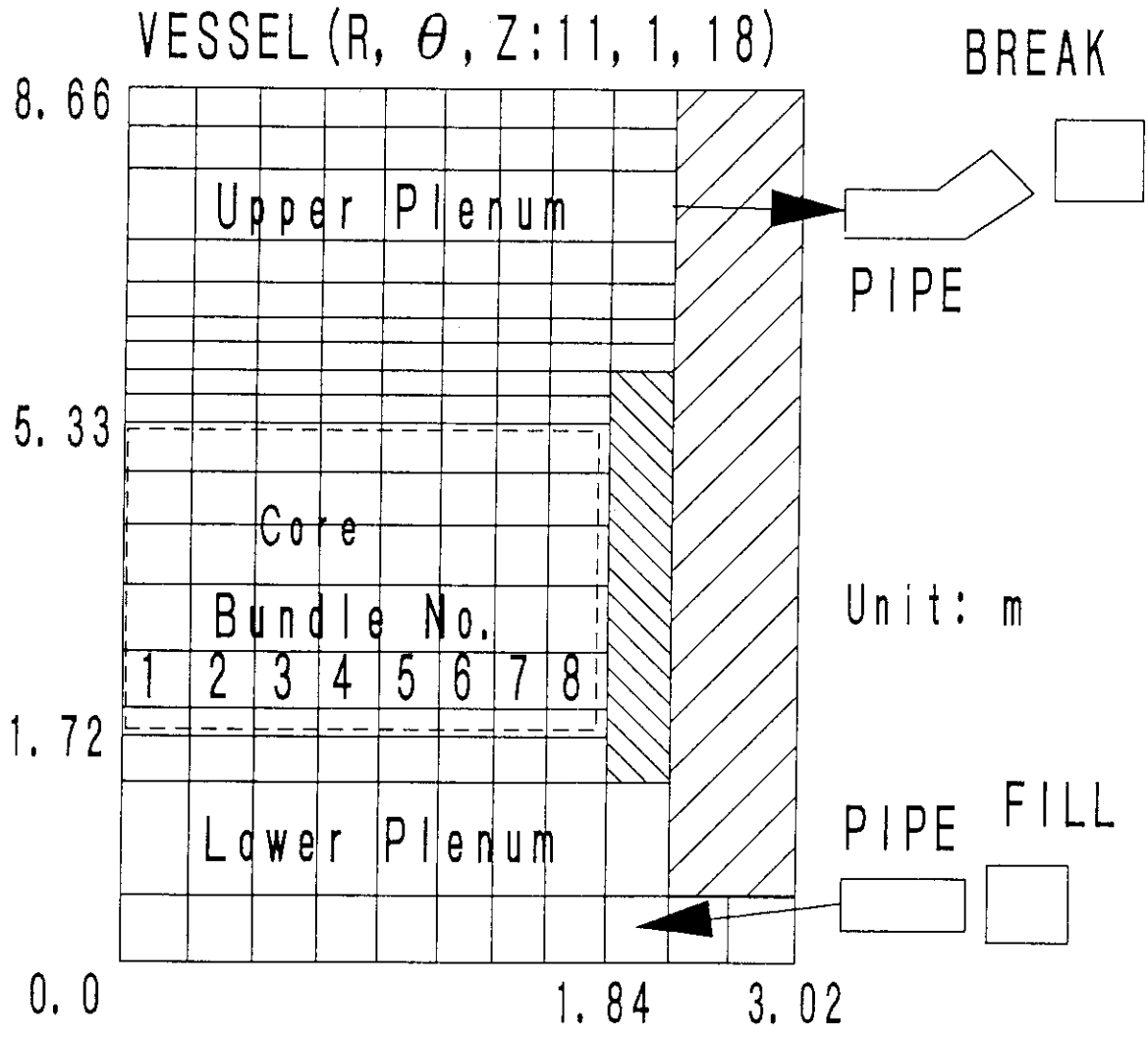

Fig. 3.1.1 Noding model for SCTF pressure vessel

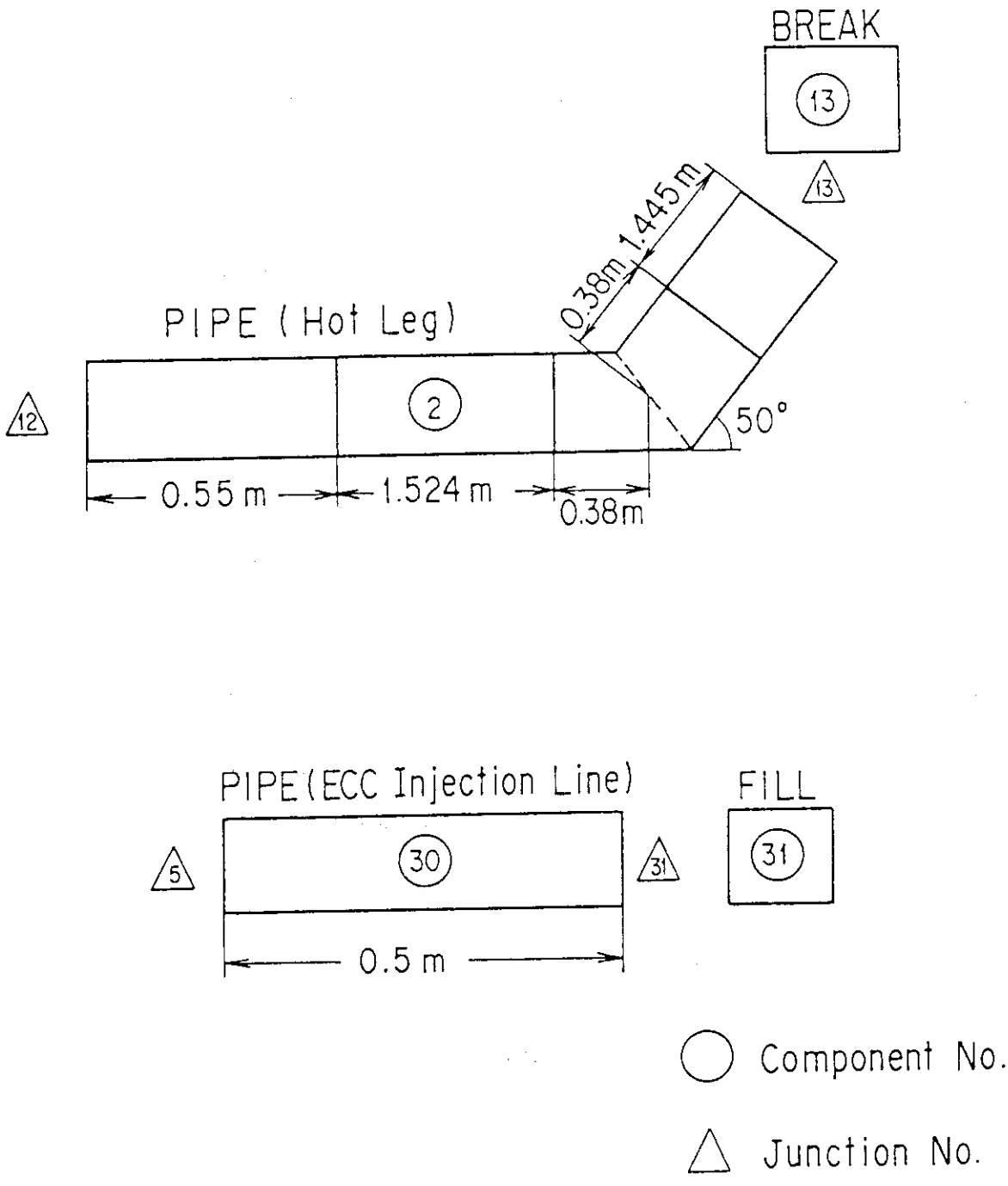

Fig. 3.1.2 Noding model for hot leg and for ECC injection line

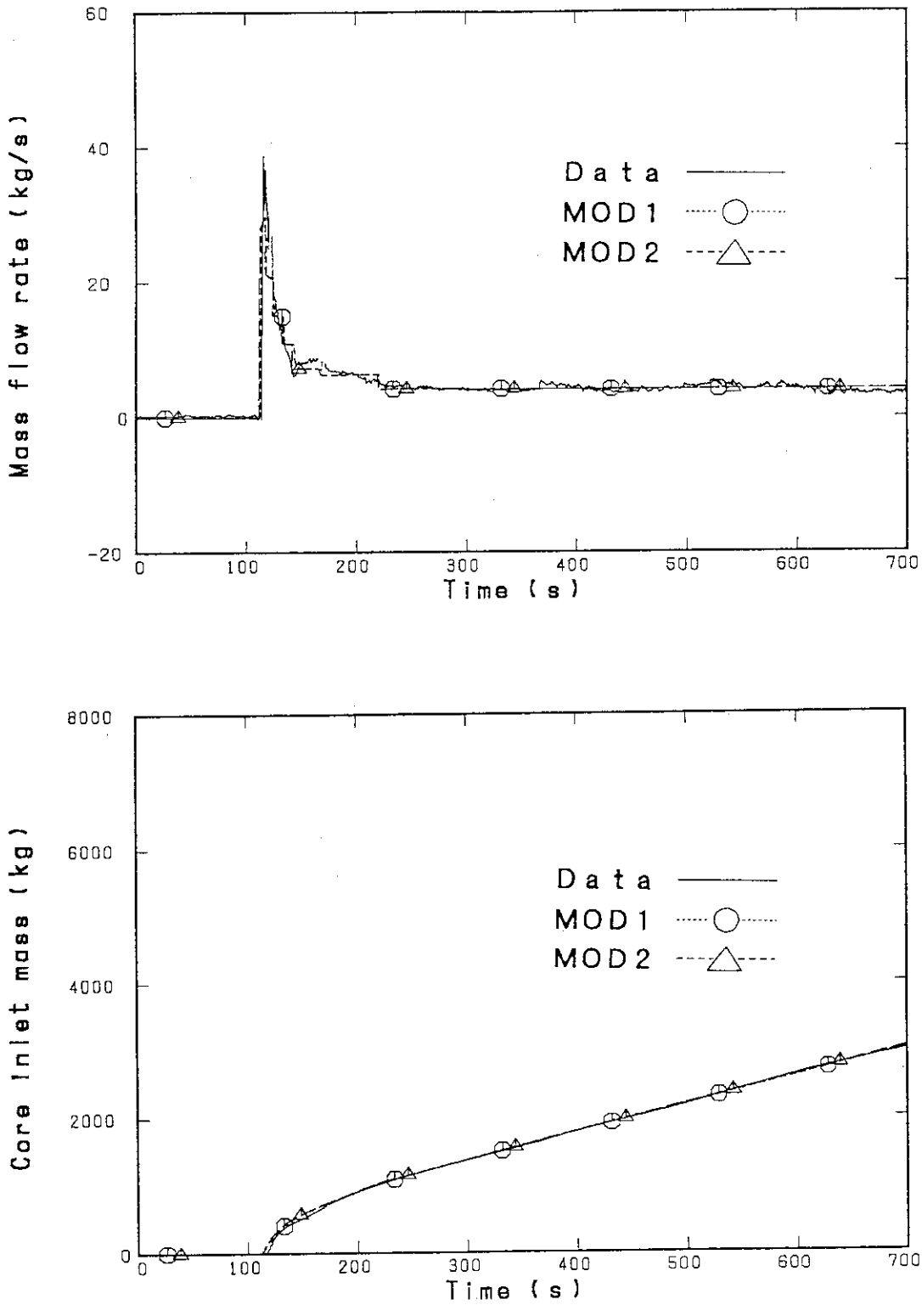

Fig. 3.2.1 Comparison of liquid mass flow rate (upper figure) and integrated liquid mass (lower figure) at core inlet

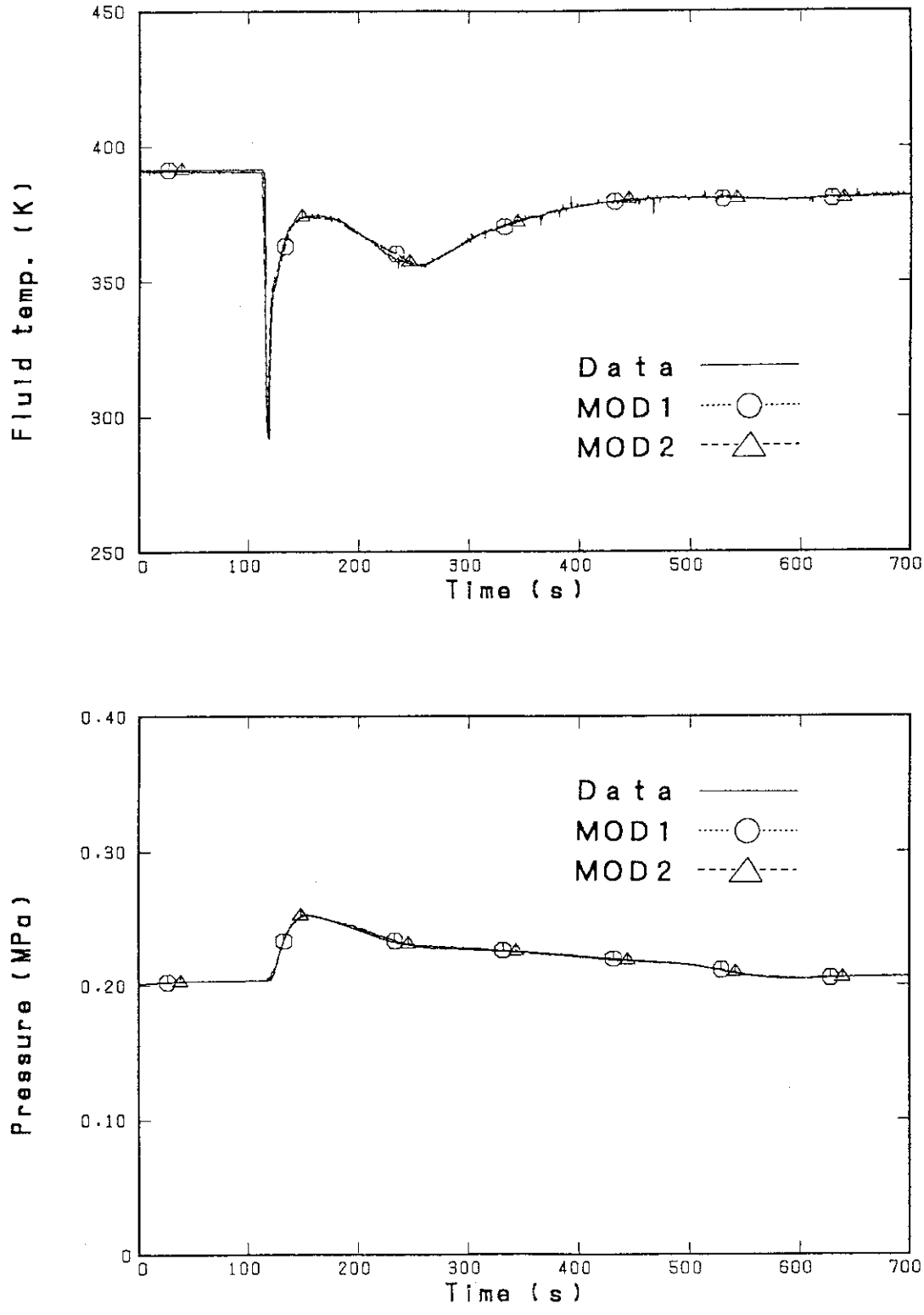

Fig. 3.2.2 Comparison of ECC water temperature (upper figure) and pressure at exit of hot leg (lower figure)

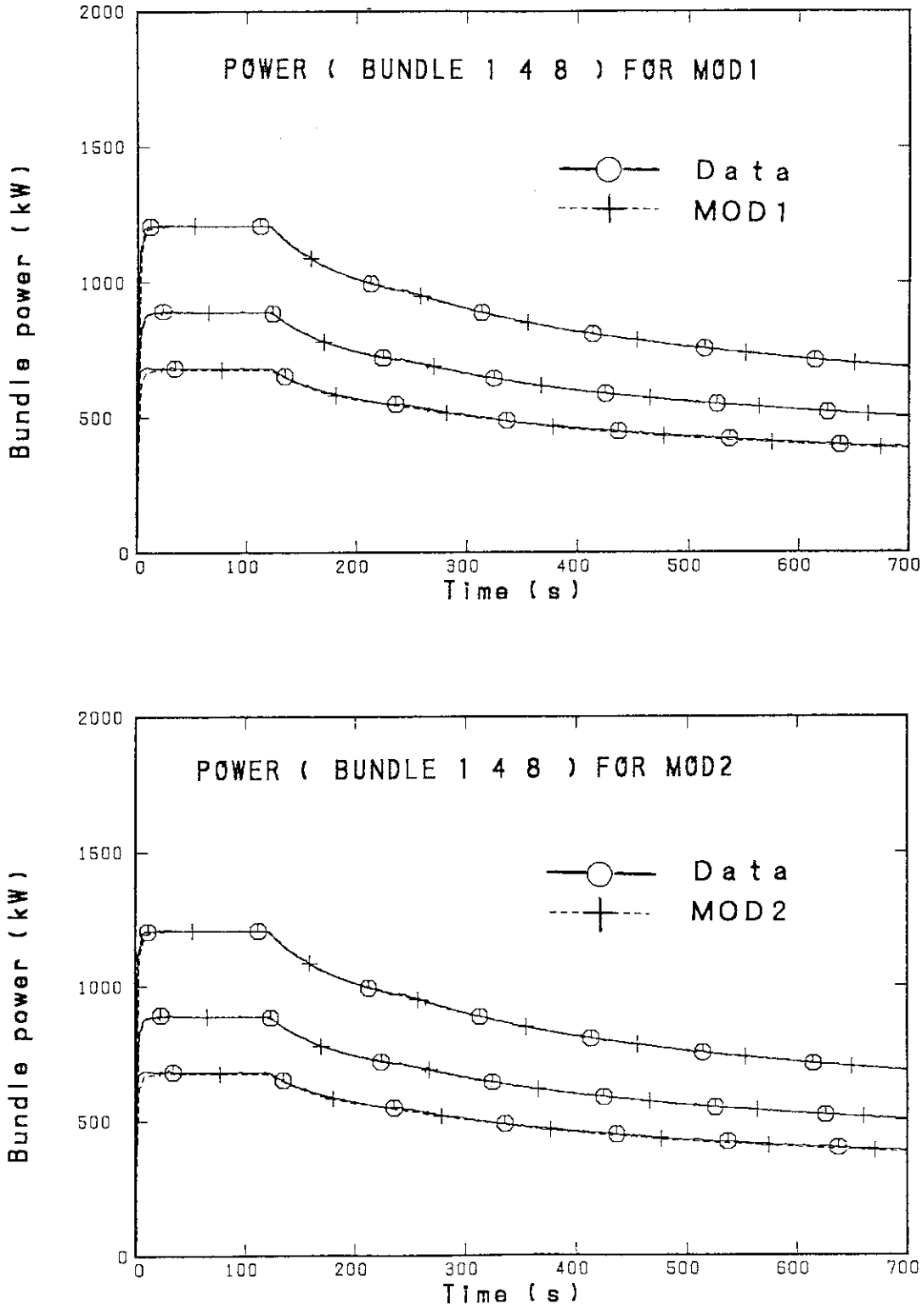

Fig. 3.2.3 Comparison of core power in calculations with TRAC-PF1/MOD1 code (upper figure) and with TRAC-PF1/MOD2 code (lower figure)

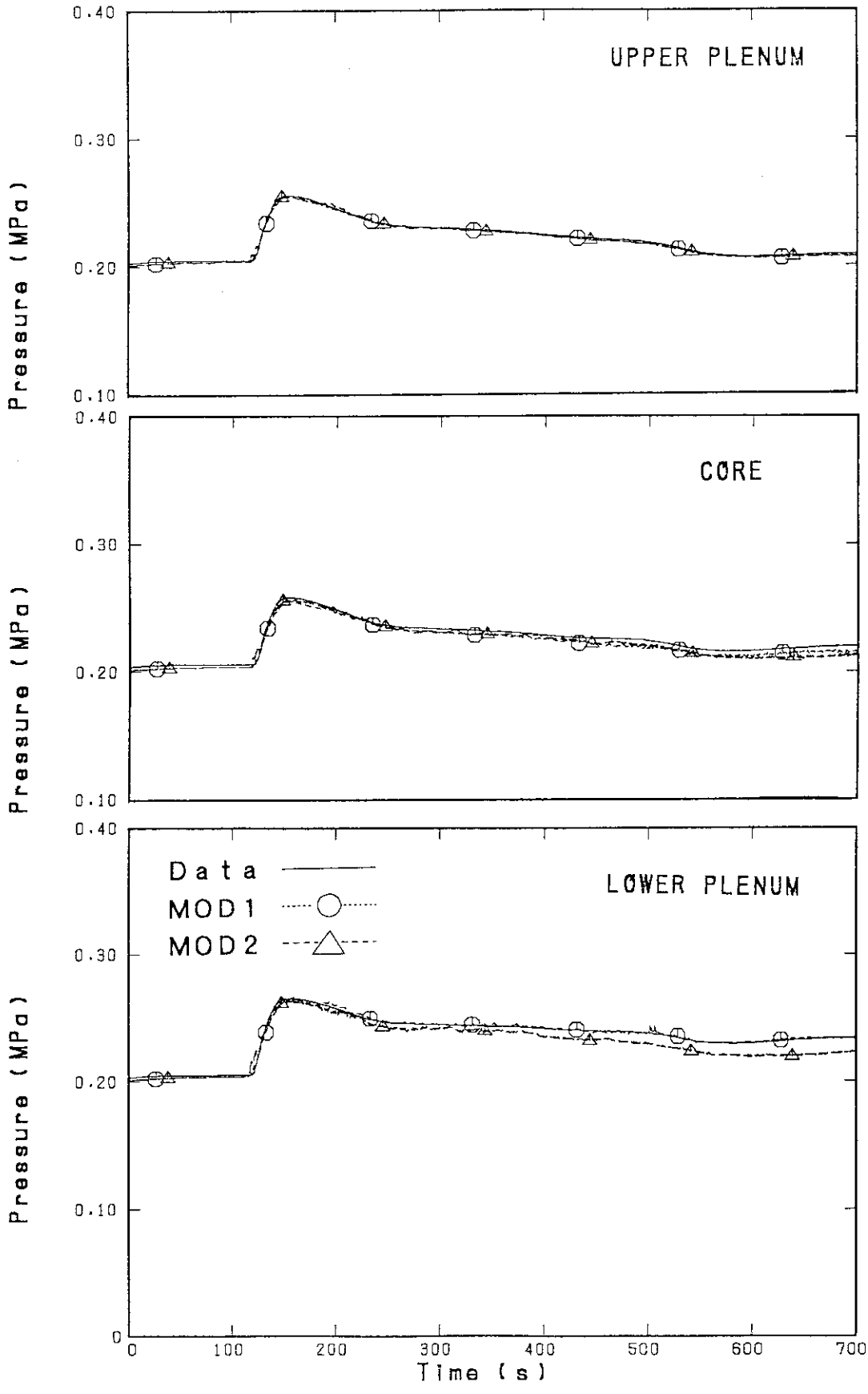

Fig. 4.1.1 Comparison of pressure in pessure vessel

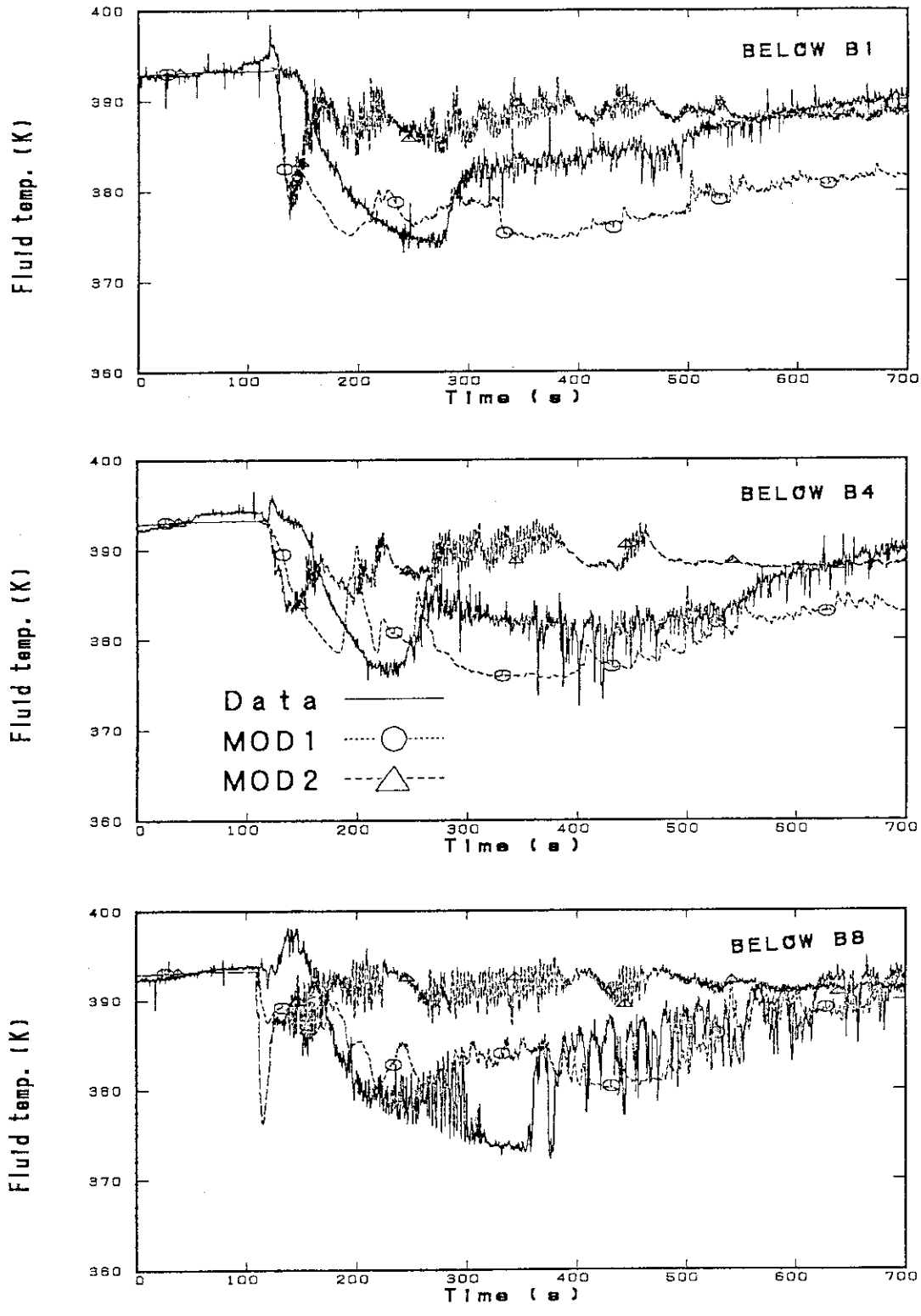

Fig. 4.1.2 Comparison of fluid temperature at core inlet below bundles 1, 4 and 8

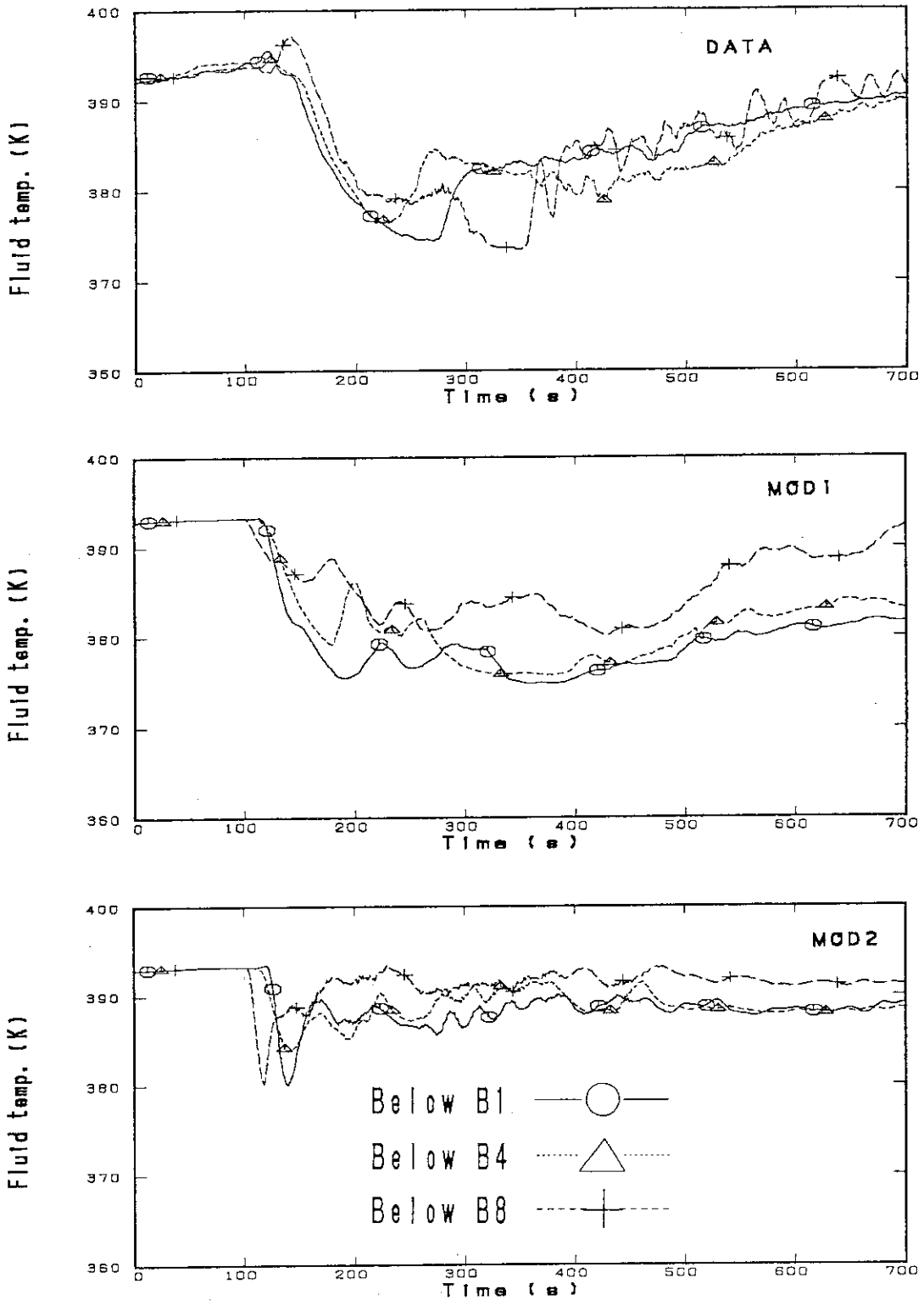

Fig. 4.1.3 Comparison of radial distribution of fluid temperature at core inlet

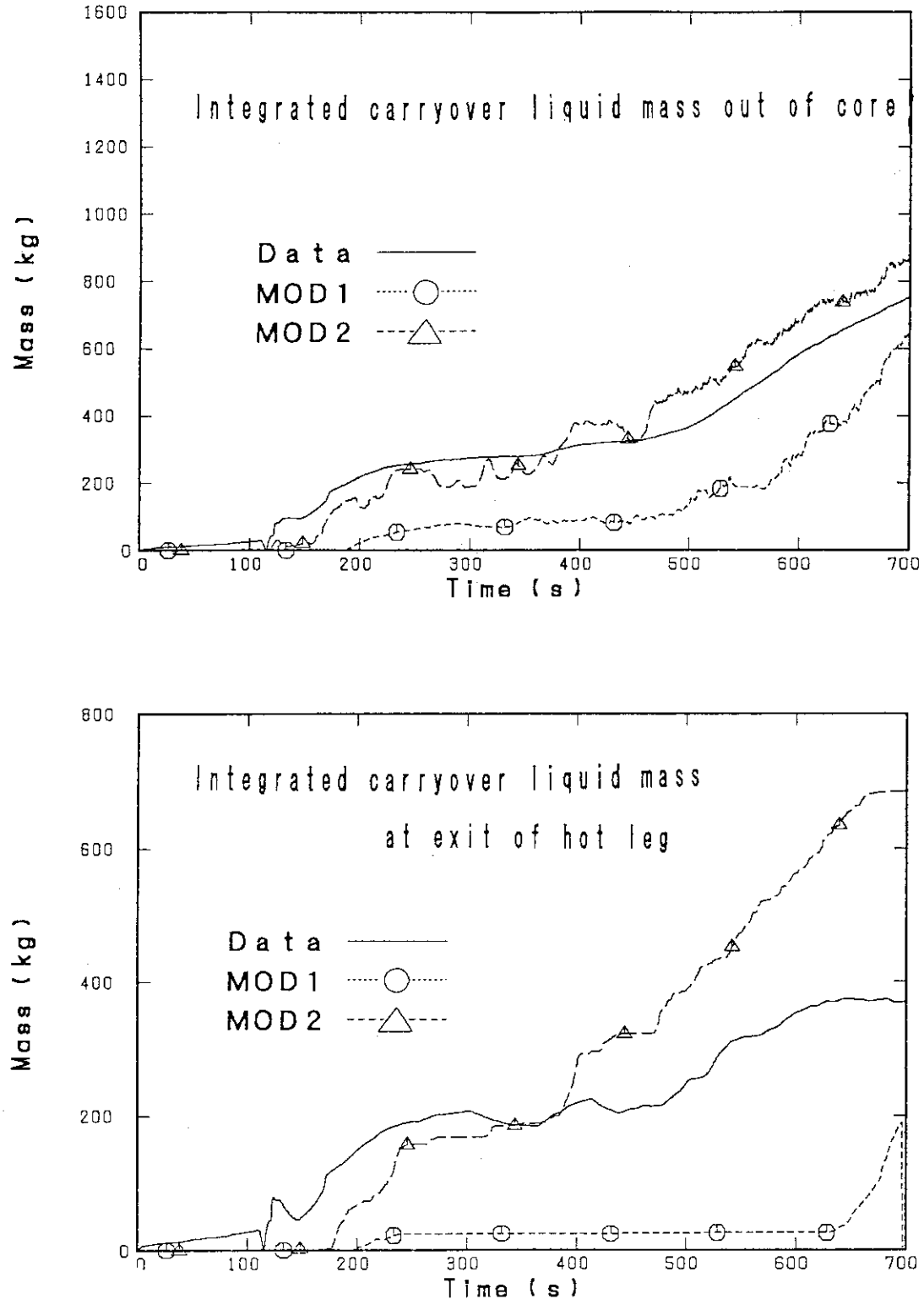

Fig. 4.1.4 Comparison of integrated carry-over liquid mass out of core (upper figure) and at exit of hot leg (lower figure)

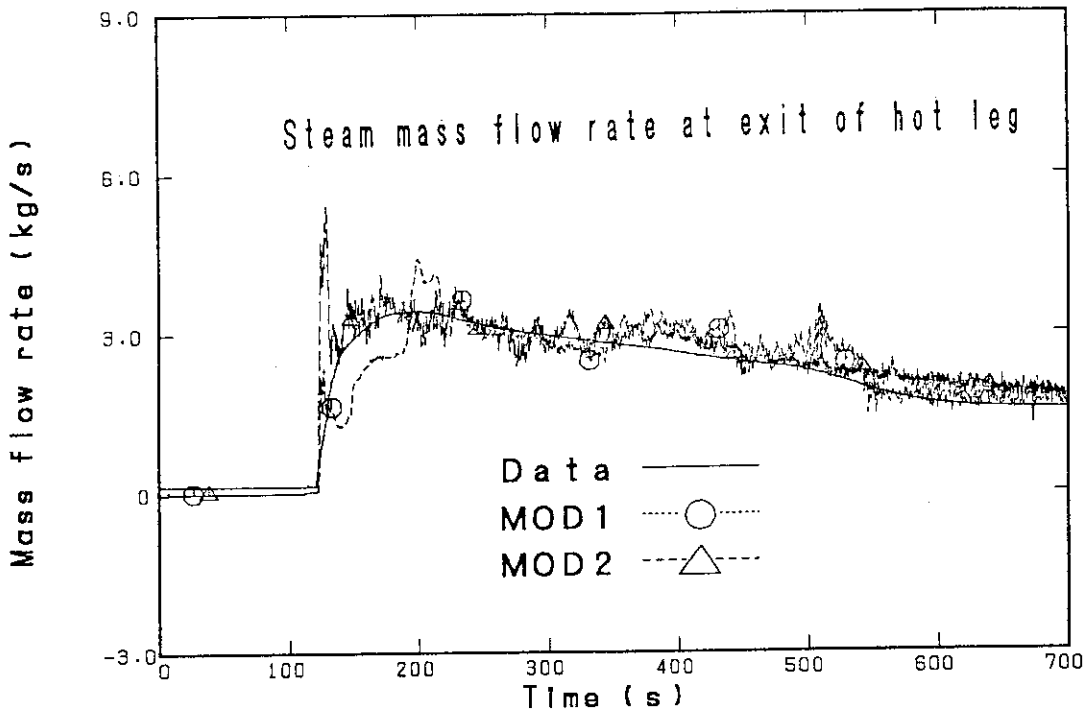

Fig. 4.1.5 Comparison of steam mass flow rate at exit of hot leg

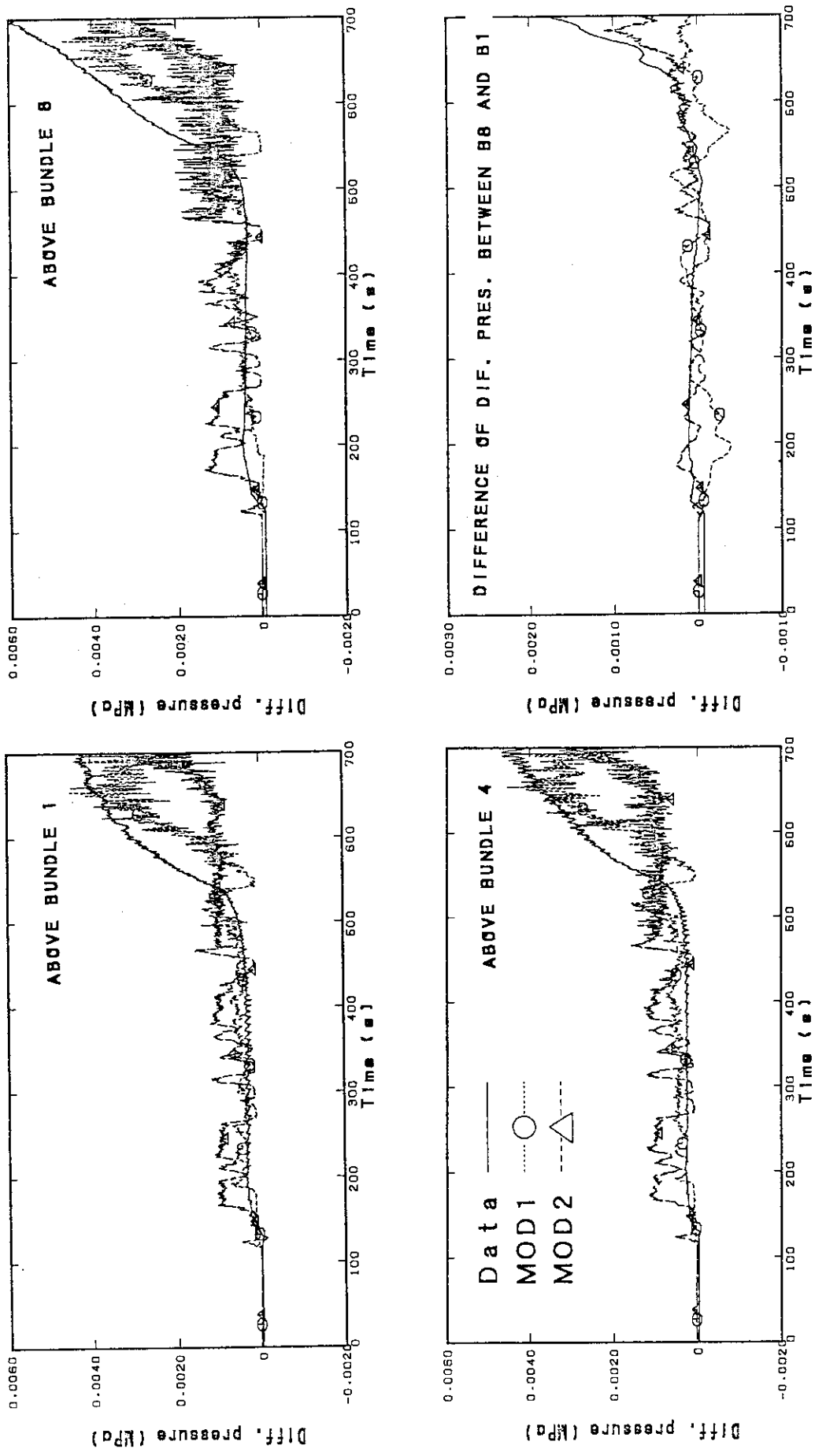

Fig. 4.1.6 Comparison of differential pressure in upper plenum

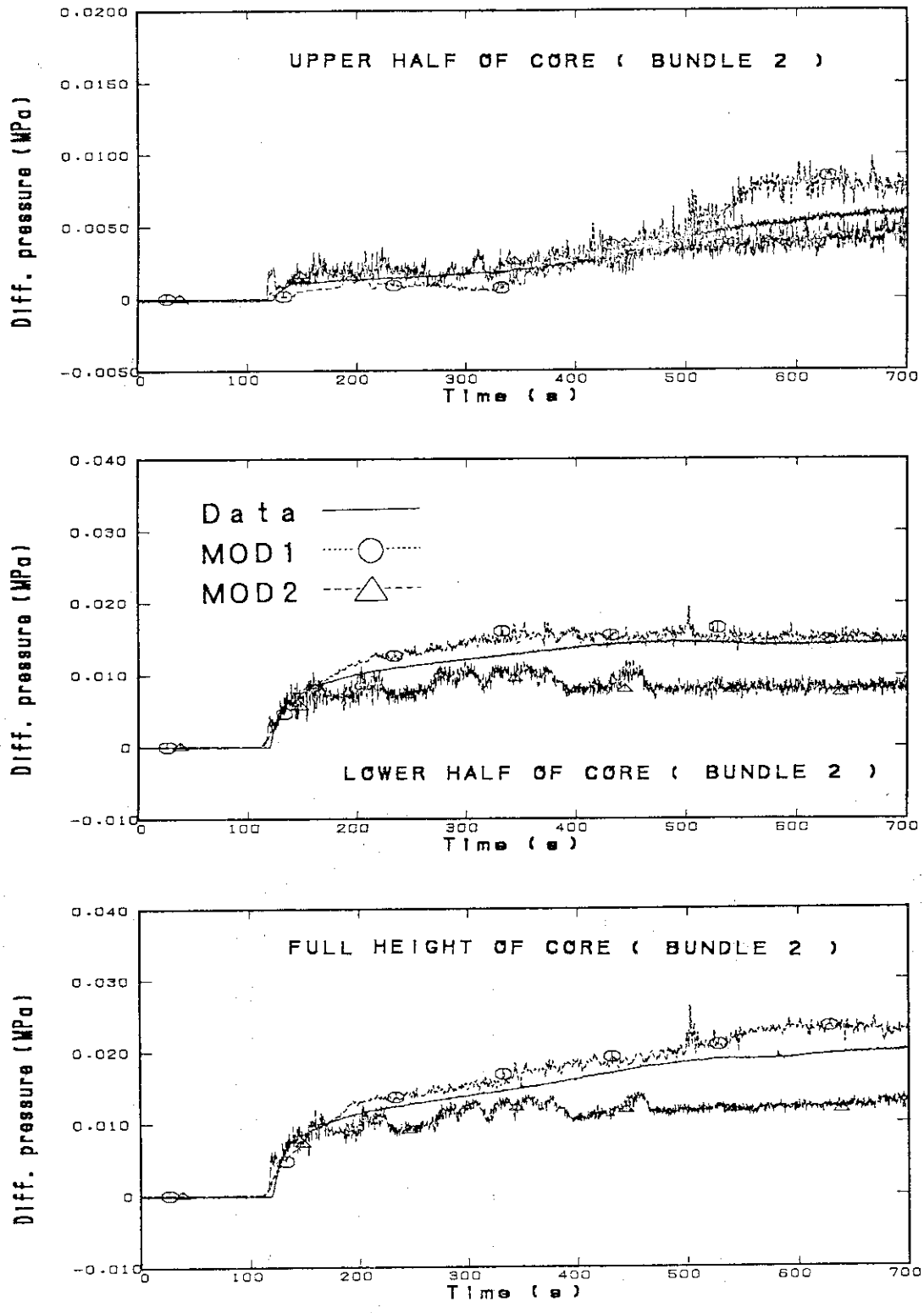

Fig. 4.2.1 Comparison of core differential pressure in bundle 2 (high power bundle)

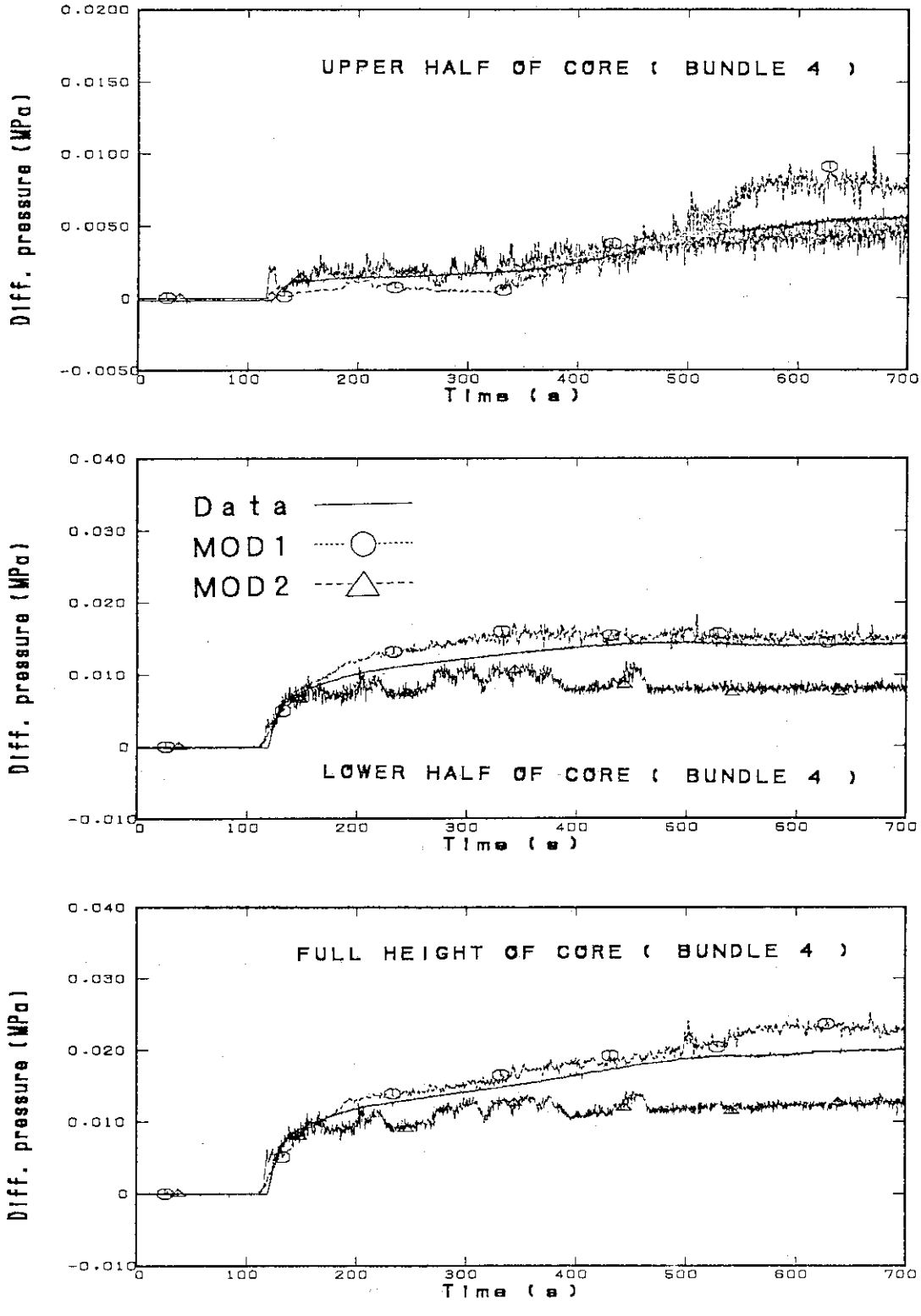

Fig. 4.2.2 Comparison of core differential pressure in bundle 4 (middle power bundle)

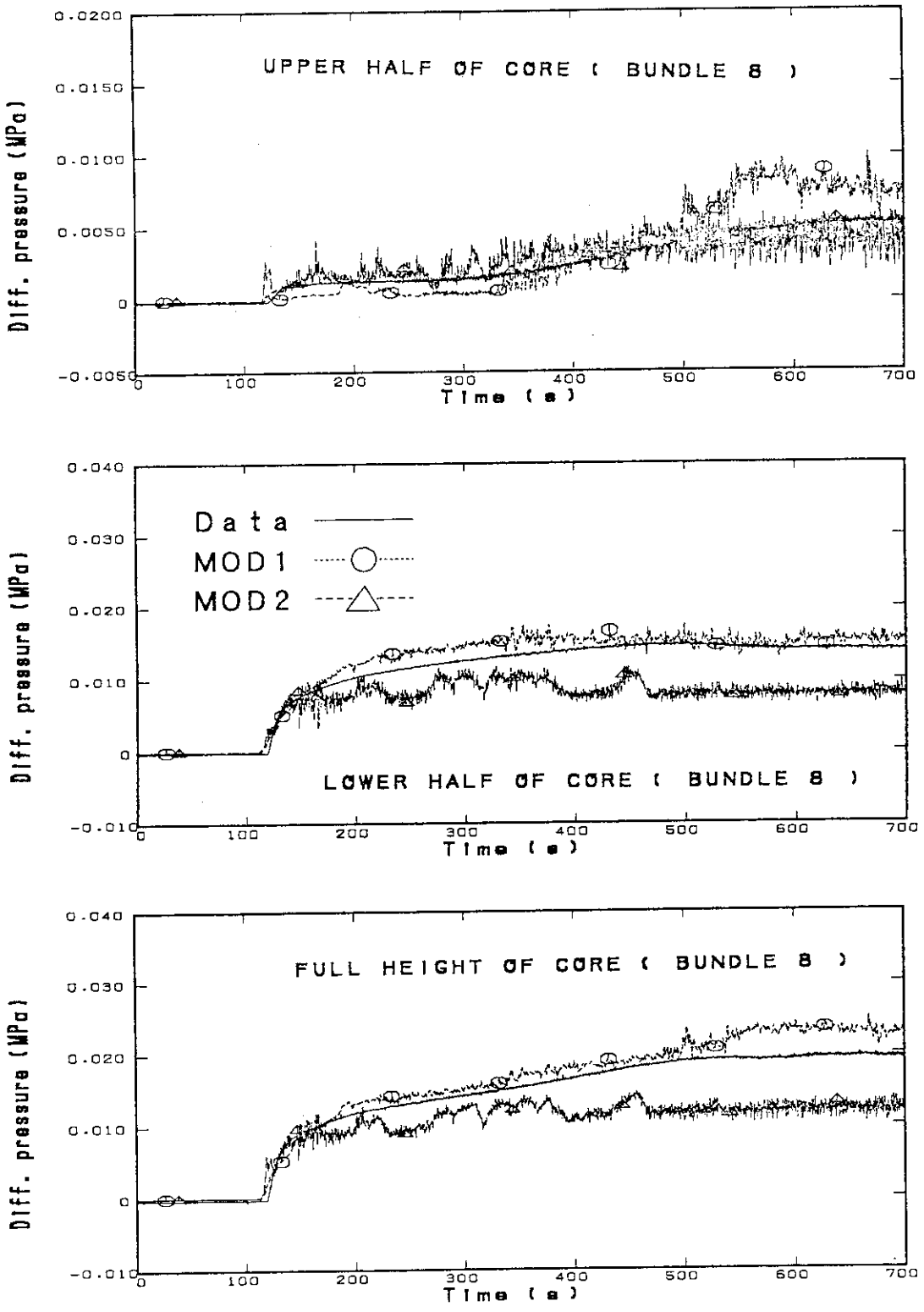

Fig. 4.2.3 Comparison of core differential pressure in bundle 8 (low power bundle)

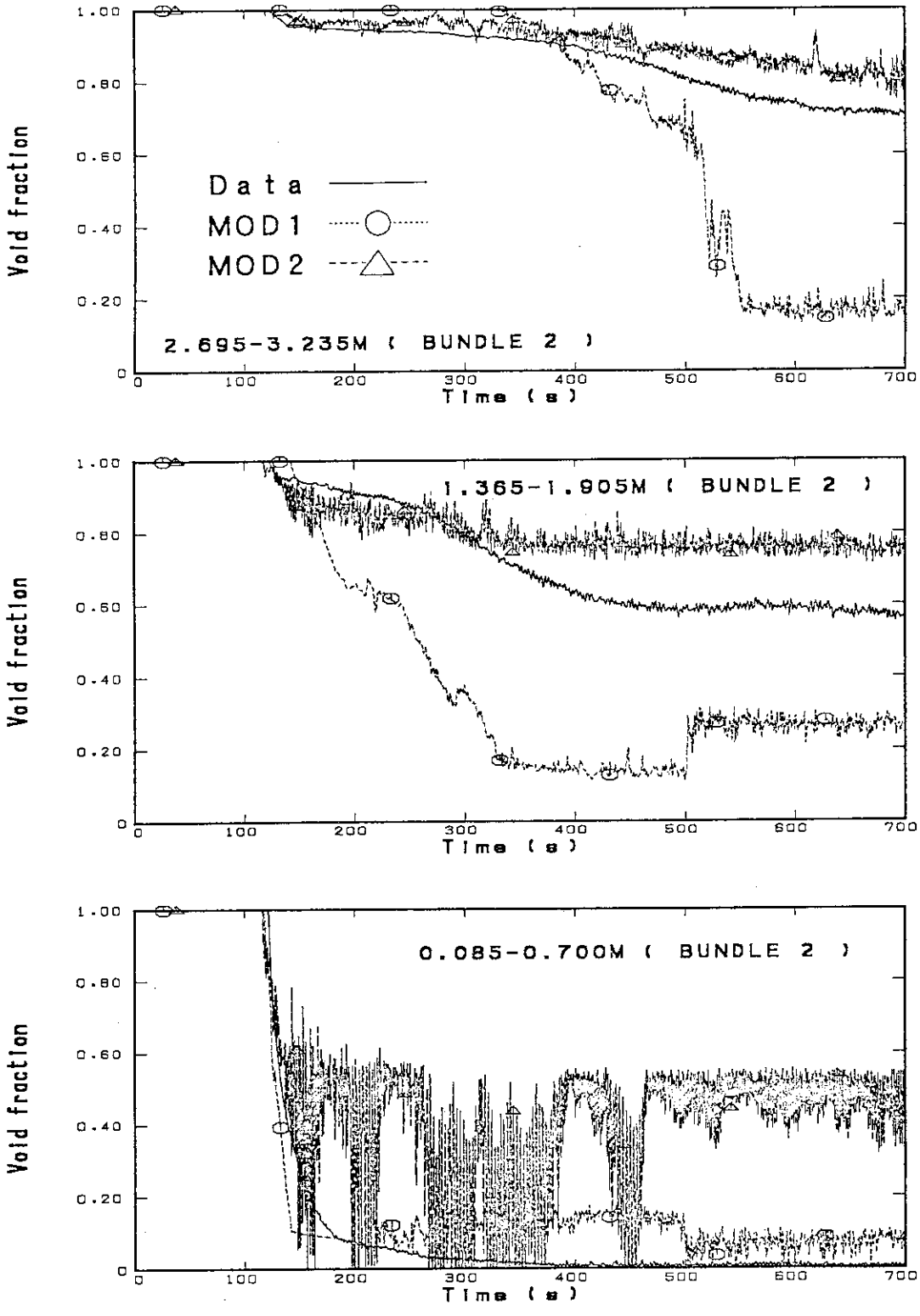

Fig. 4.2.4 Comparison of sectional void fraction in bundle 2 (high power bundle)

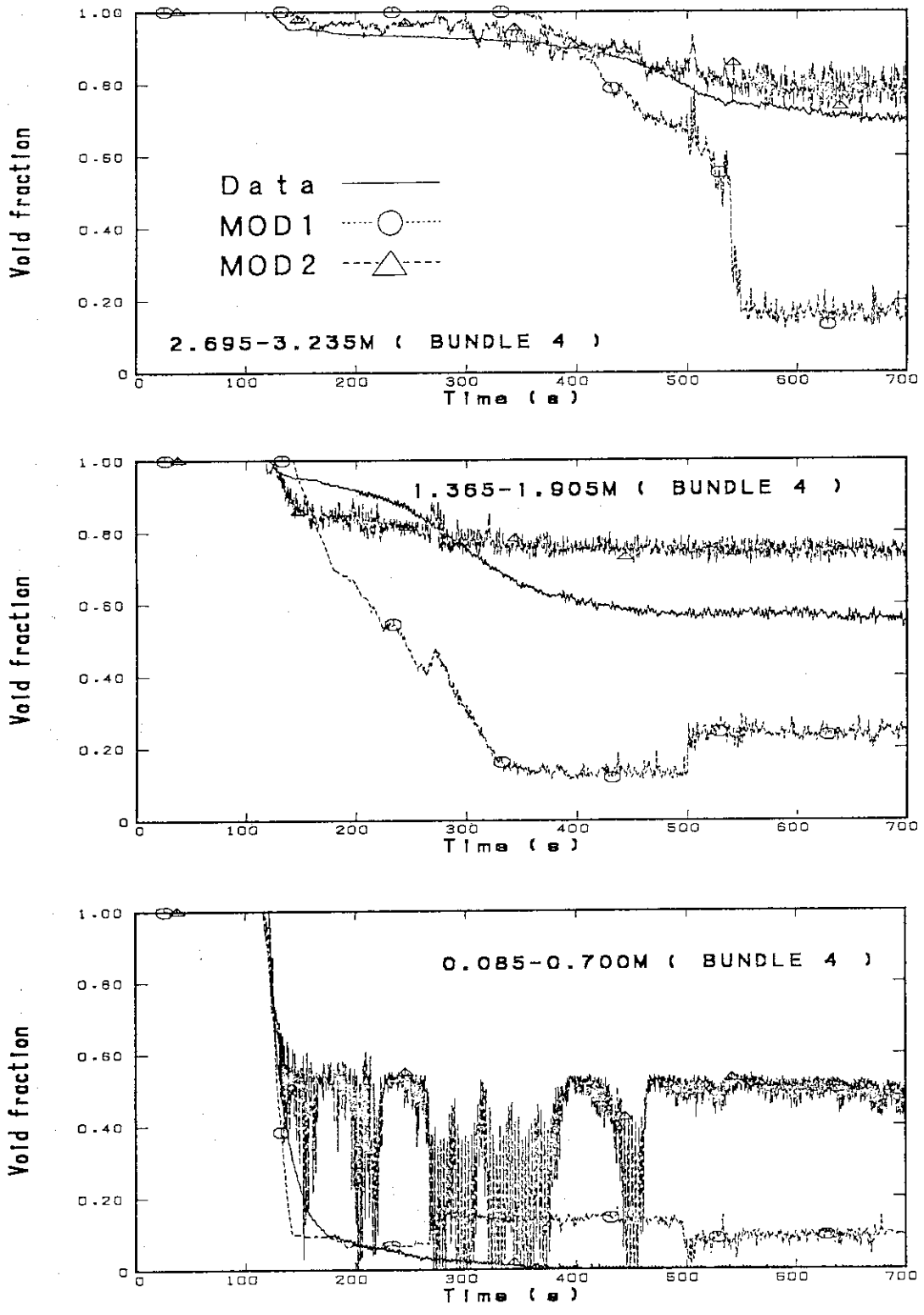

Fig. 4.2.5 Comparison of sectional void fraction in bundle 4 (middle power bundle)

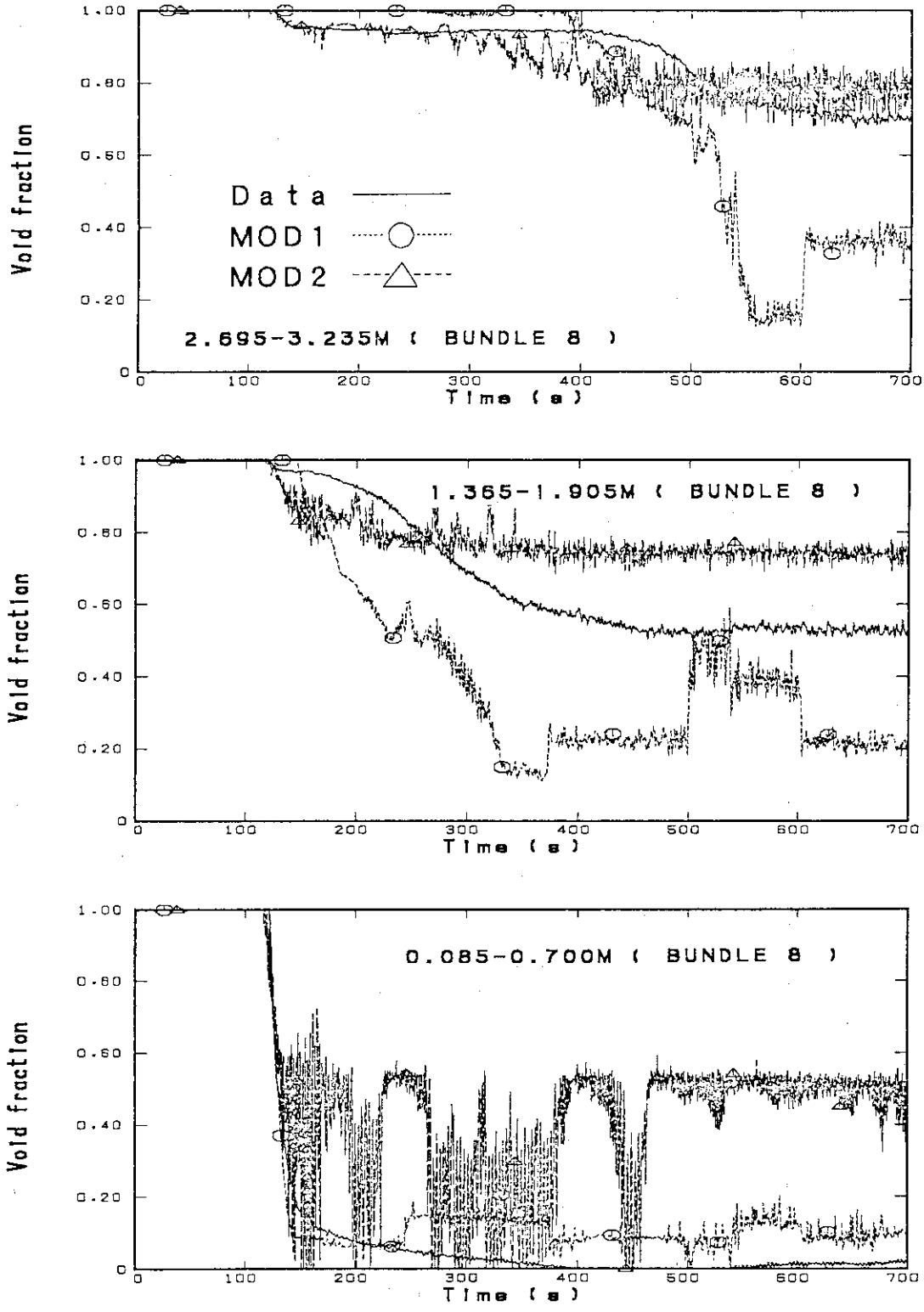

Fig. 4.2.6 Comparison of sectional void fraction in bundle 8 (low power bundle)

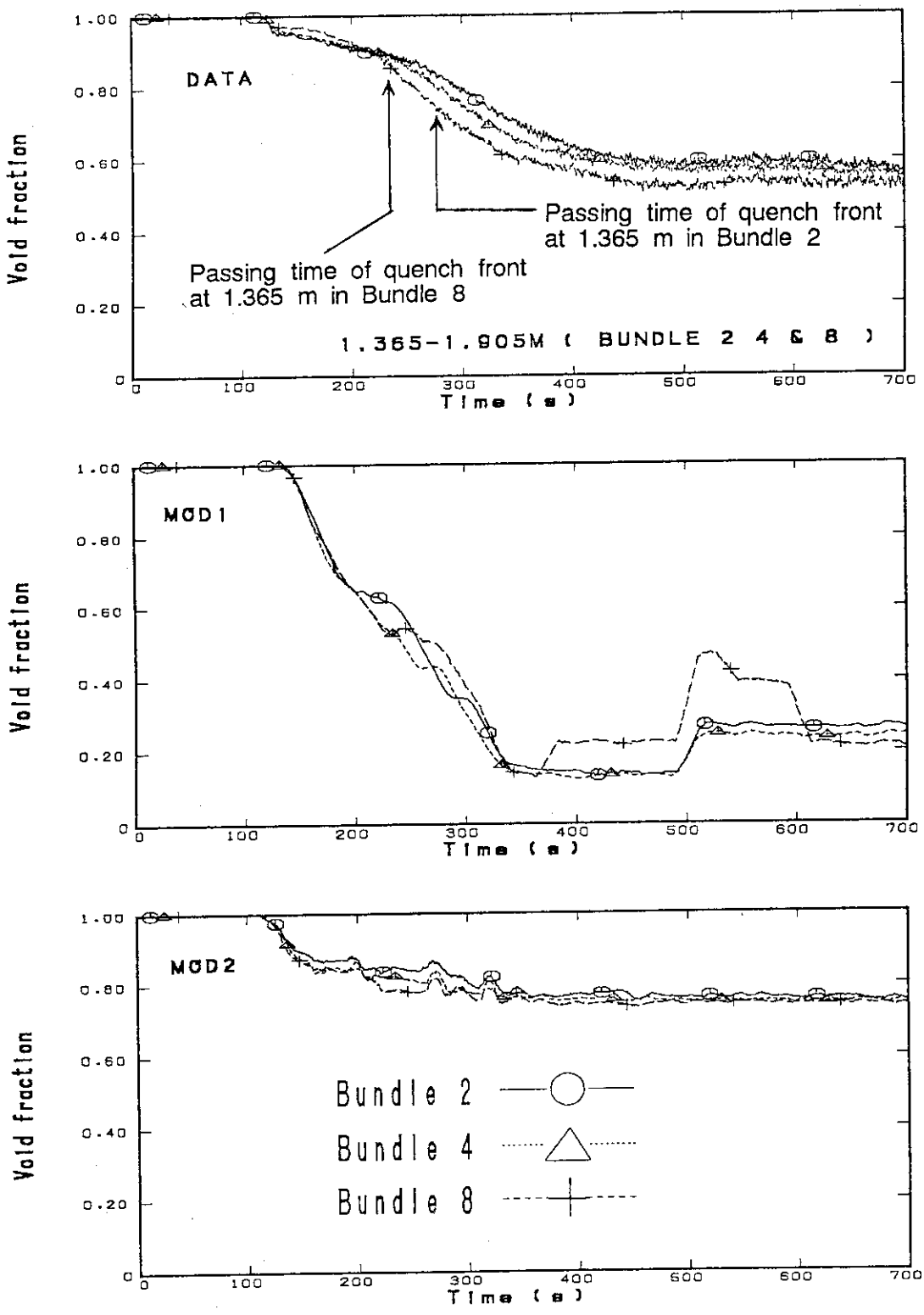

Fig. 4.2.7 Comparison of radial distribution of sectional void fraction in the region of 1.365-1.905 m

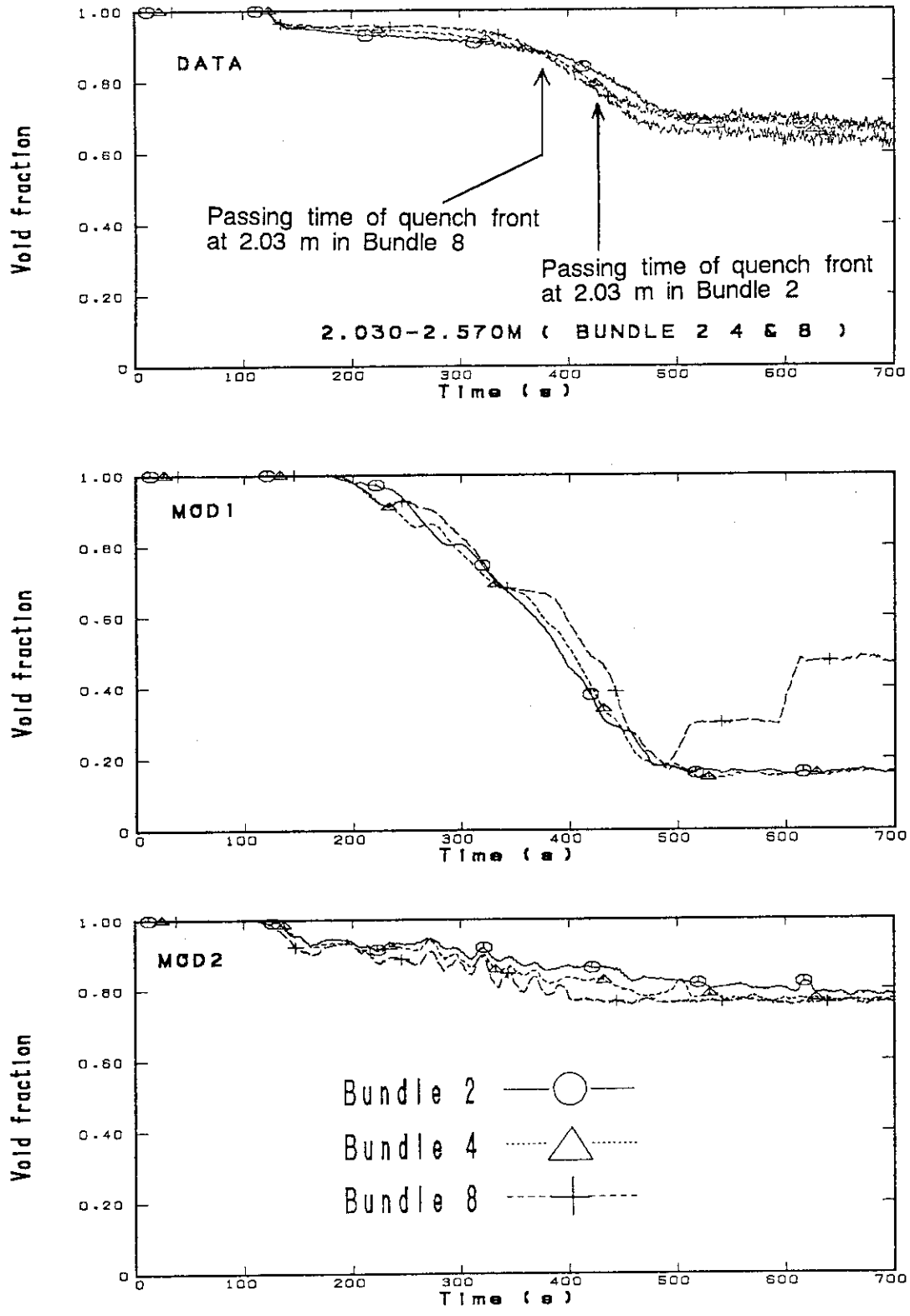

Fig. 4.2.8 Comparison of radial distribution of sectional void fraction in the region of 2.03-2.57 m

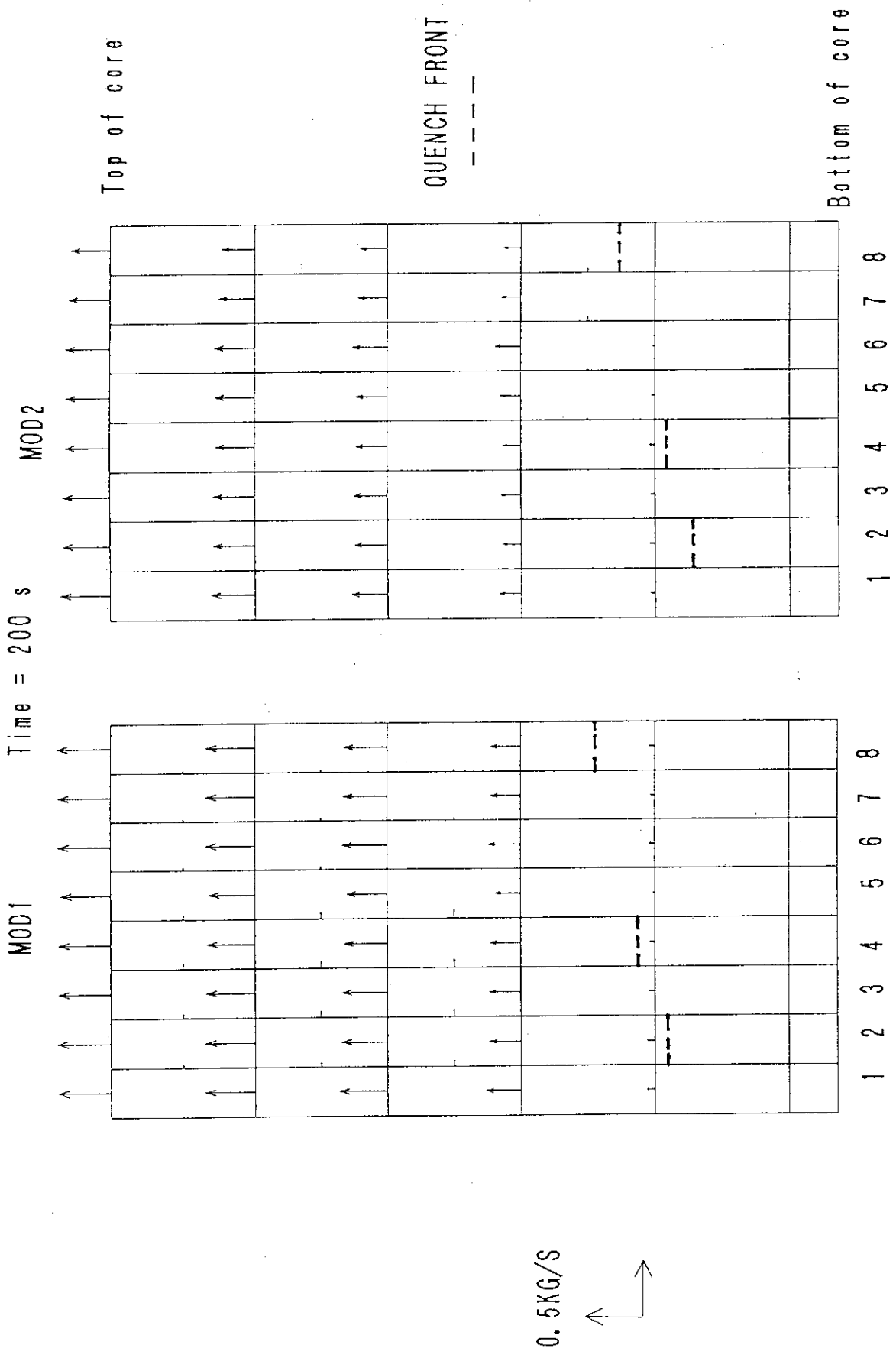

Fig. 4.2.9(1) Two-dimensional steam mass flow rate distribution in core at 200 sec

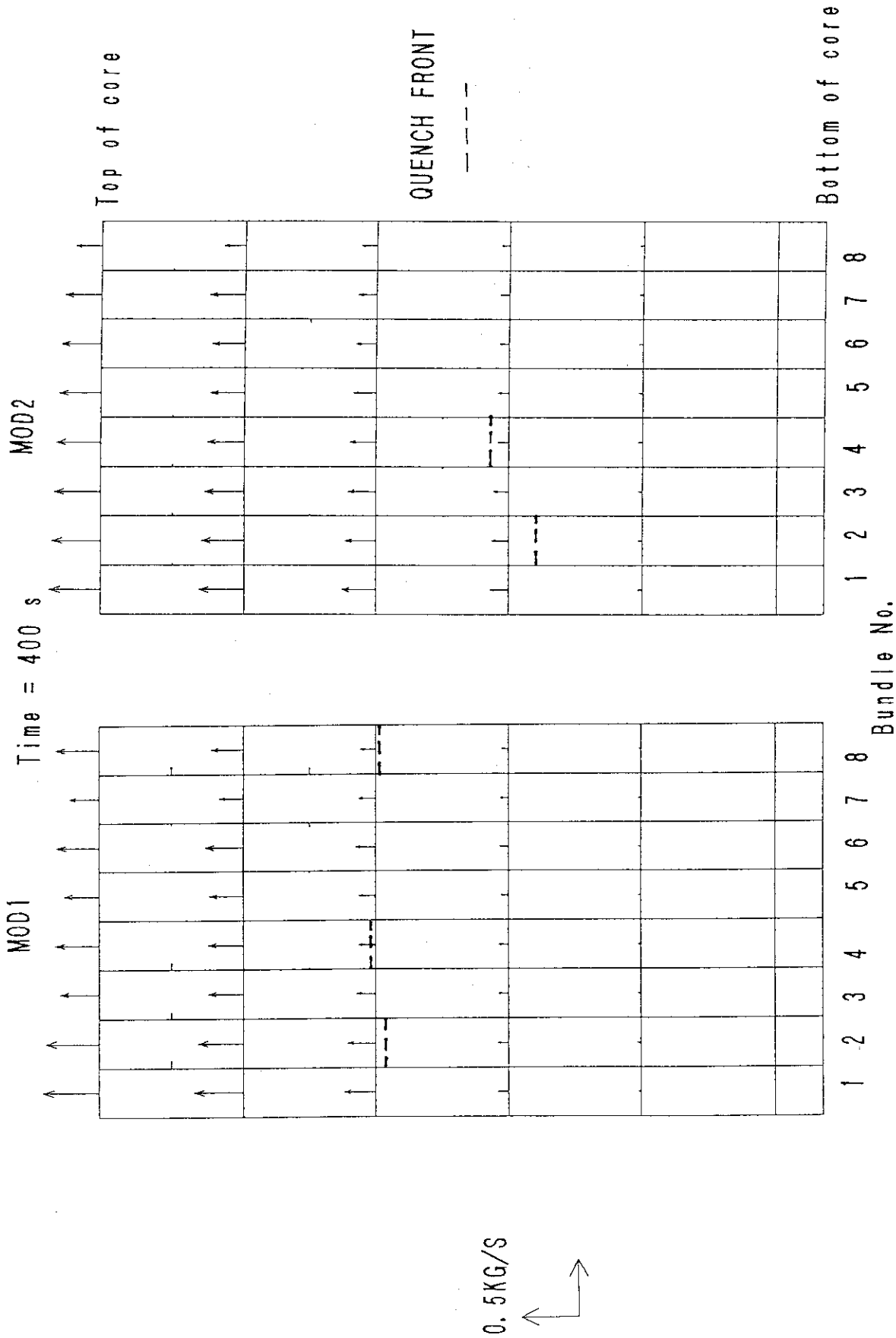

Fig. 4.2.9(2) Two-dimensional steam mass flow rate distribution in core at 400 sec

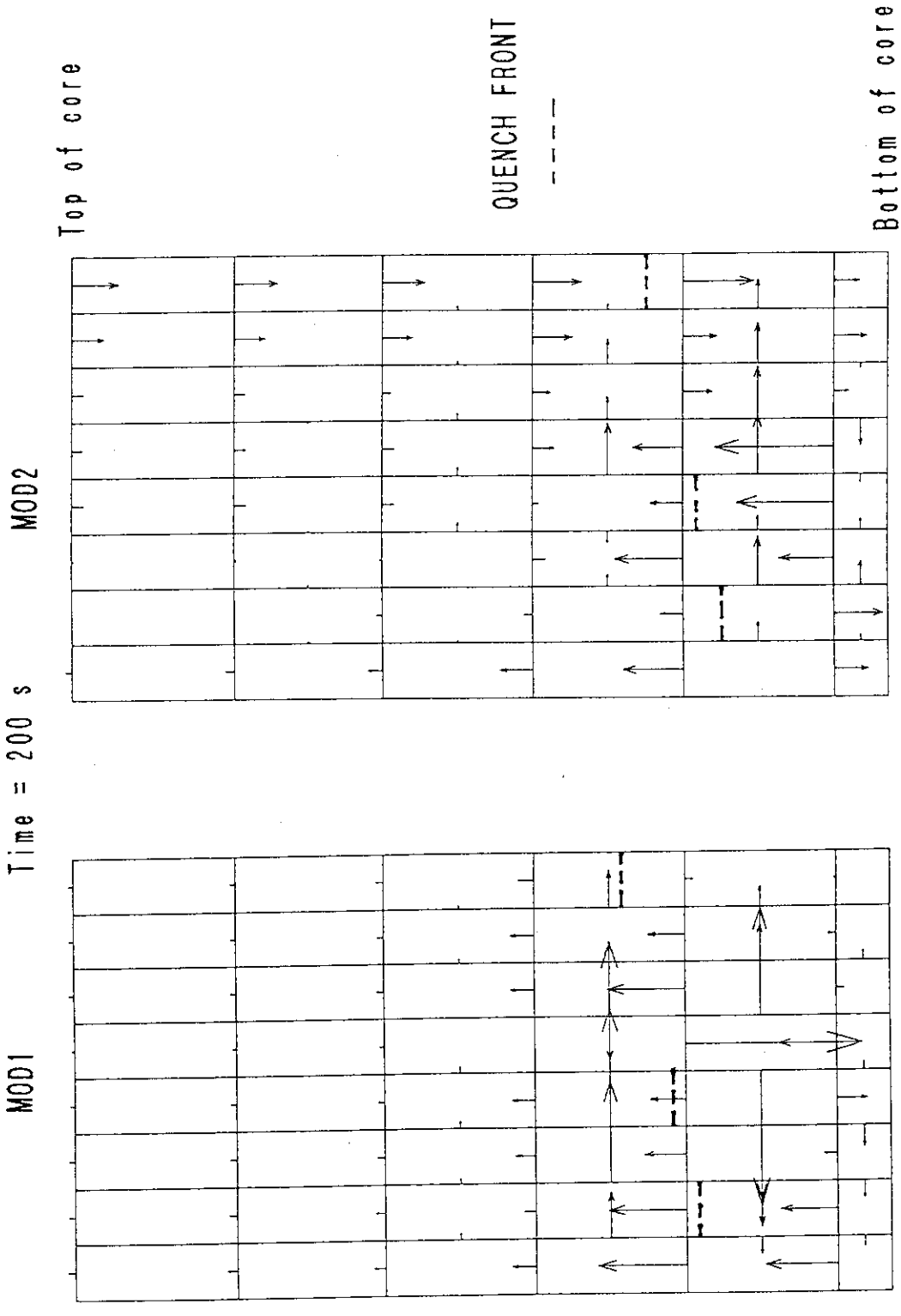

Fig. 4.2.10(1) Two-dimensional liquid mass flow rate distribution in core at 200 sec

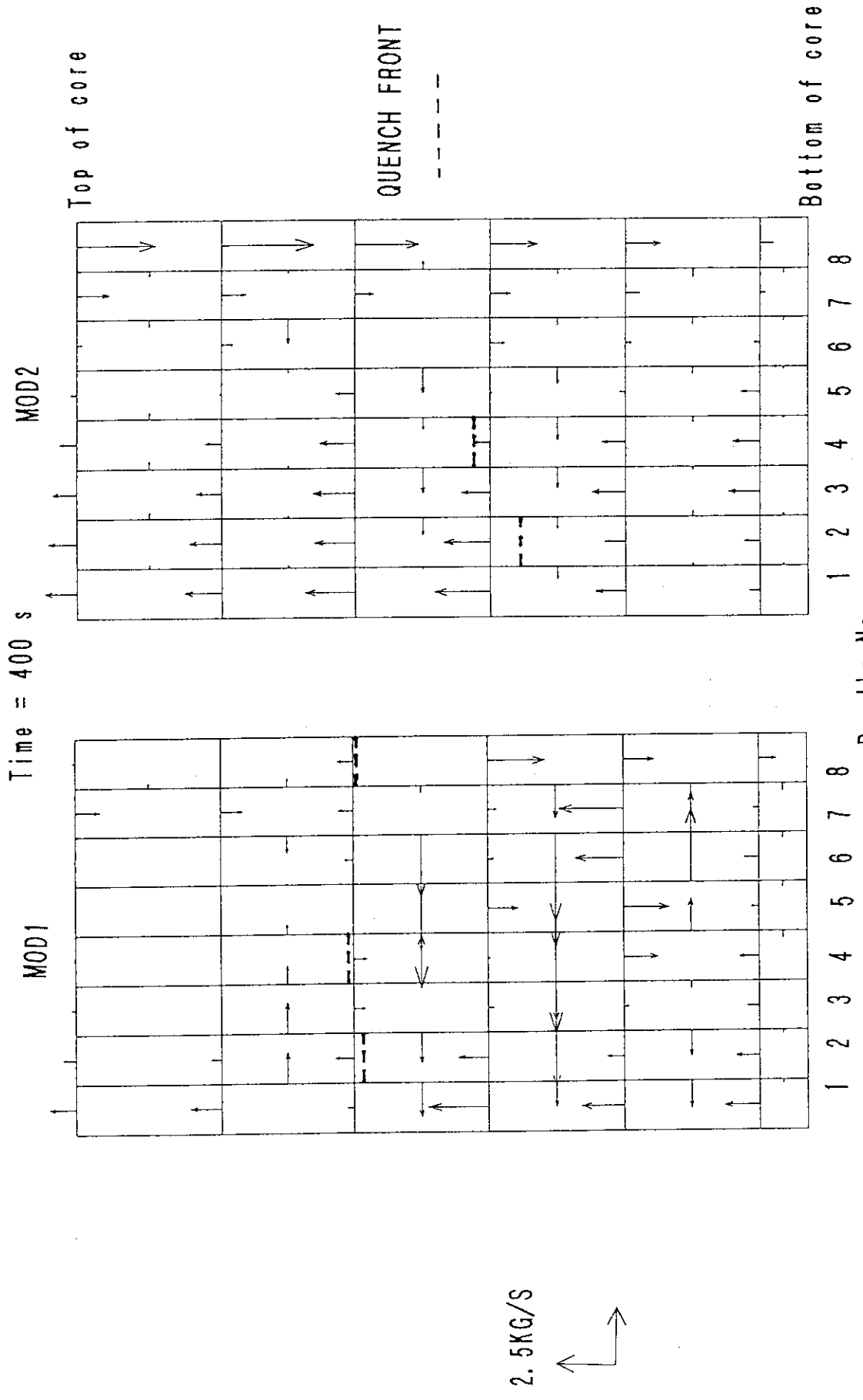

Fig. 4.2.10(2) Two-dimensional liquid mass flow rate distribution in core at 400 sec

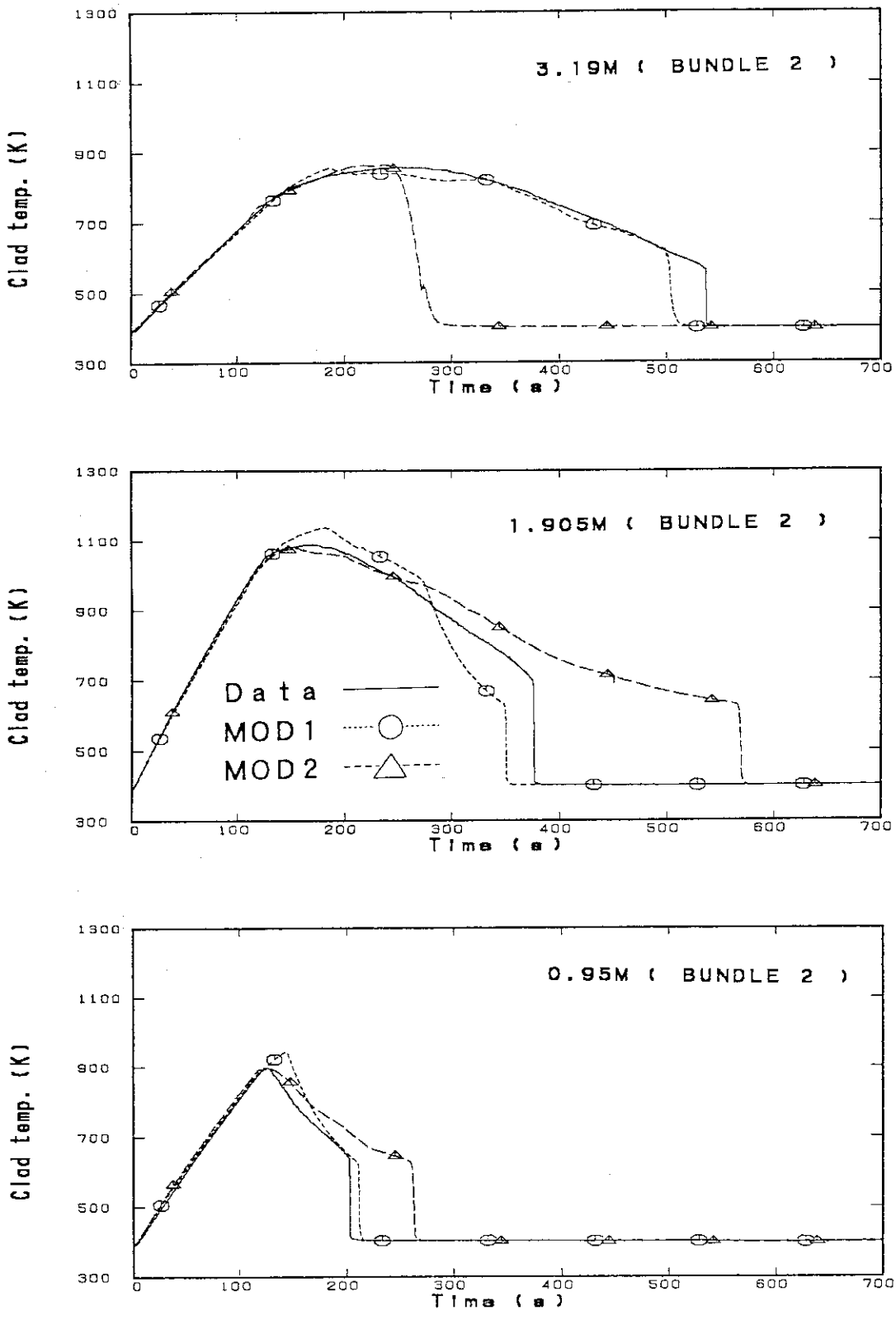

Fig. 4.3.1 Comparison of clad surface temperature in bundle 2 (high power bundle)

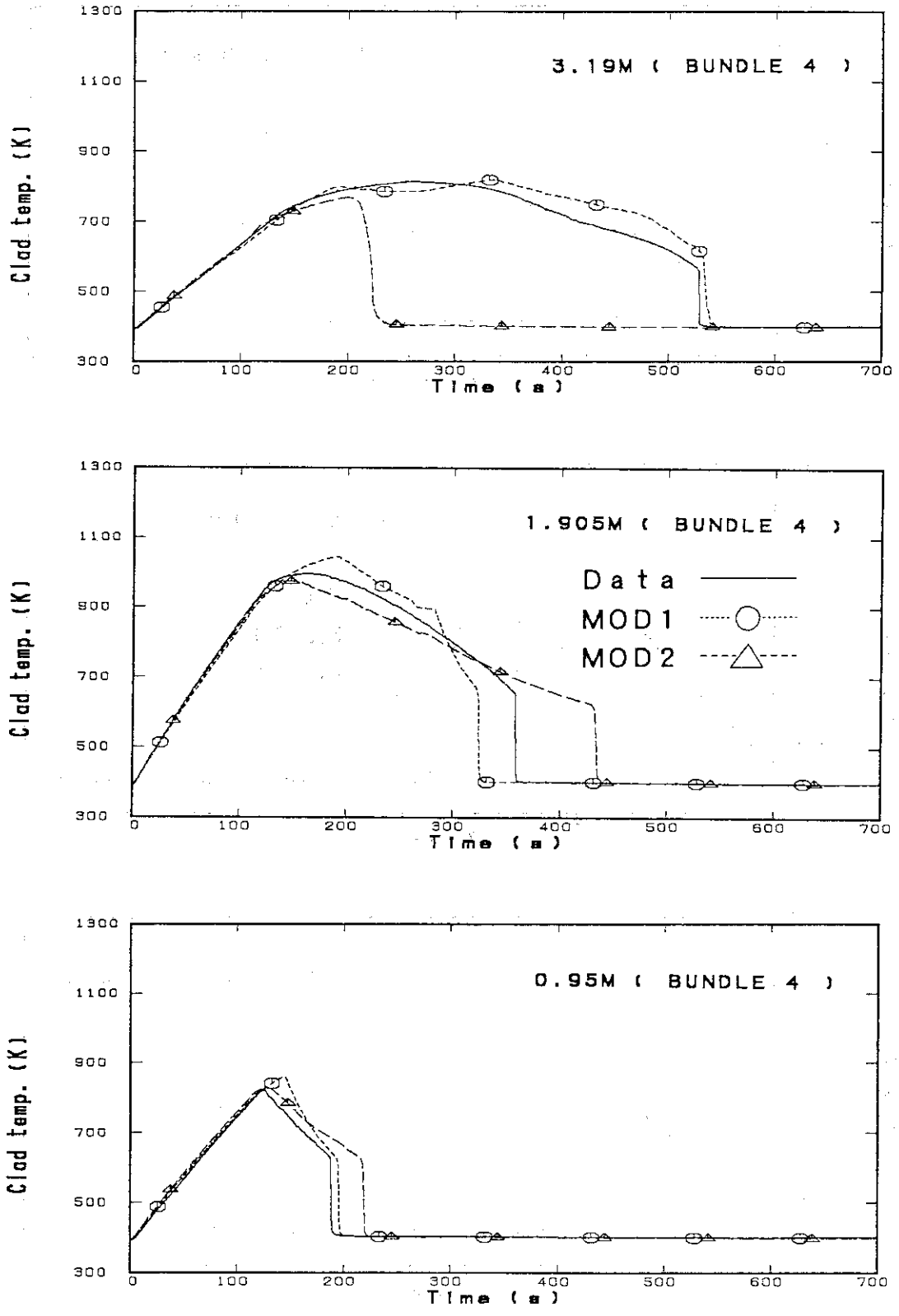

Fig. 4.3.2 Comparison of clad surface temperature in bundle 4 (middle power bundle)

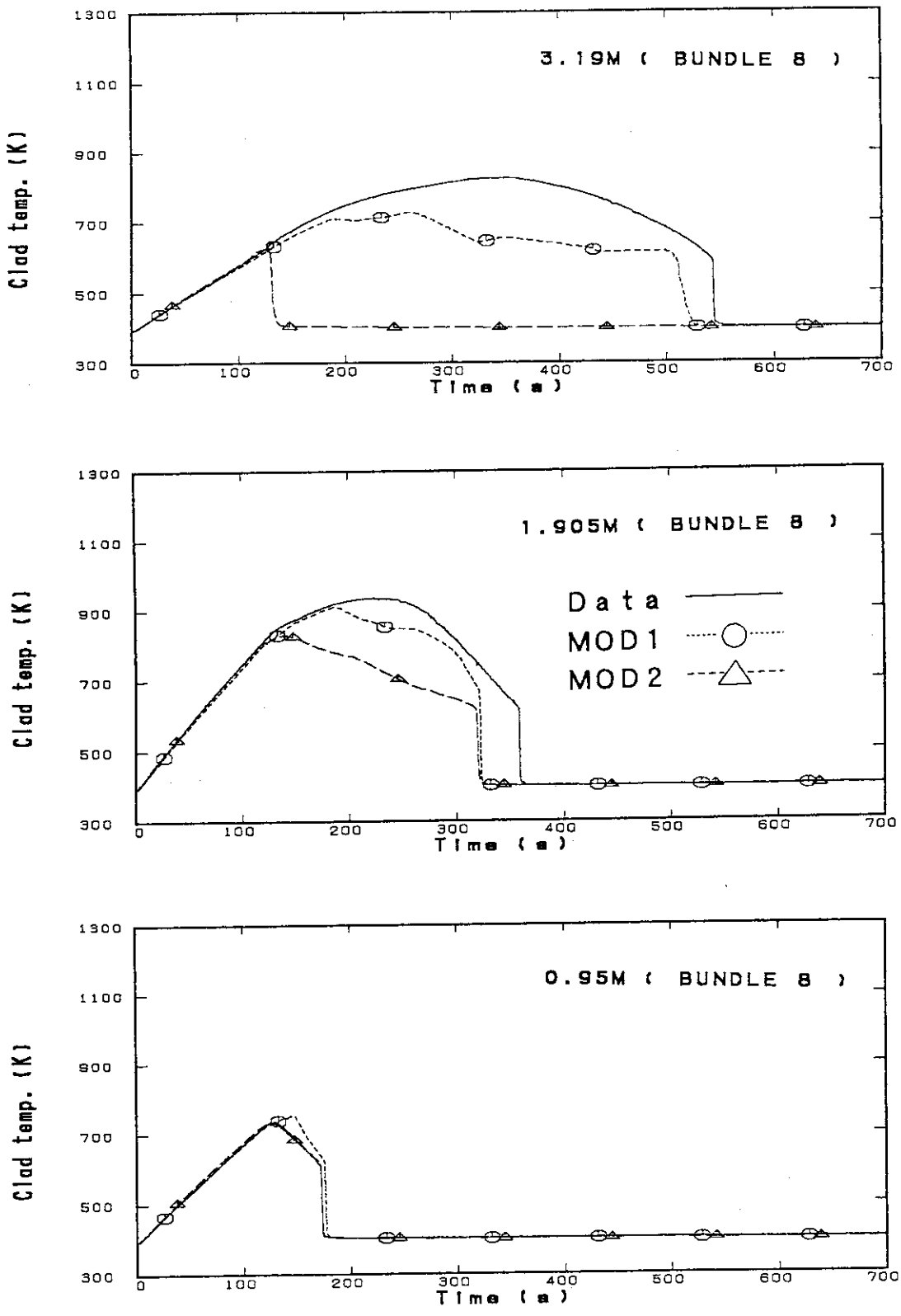

Fig. 4.3.3 Comparison of clad surface temperature in bundle 8 (low power bundle)

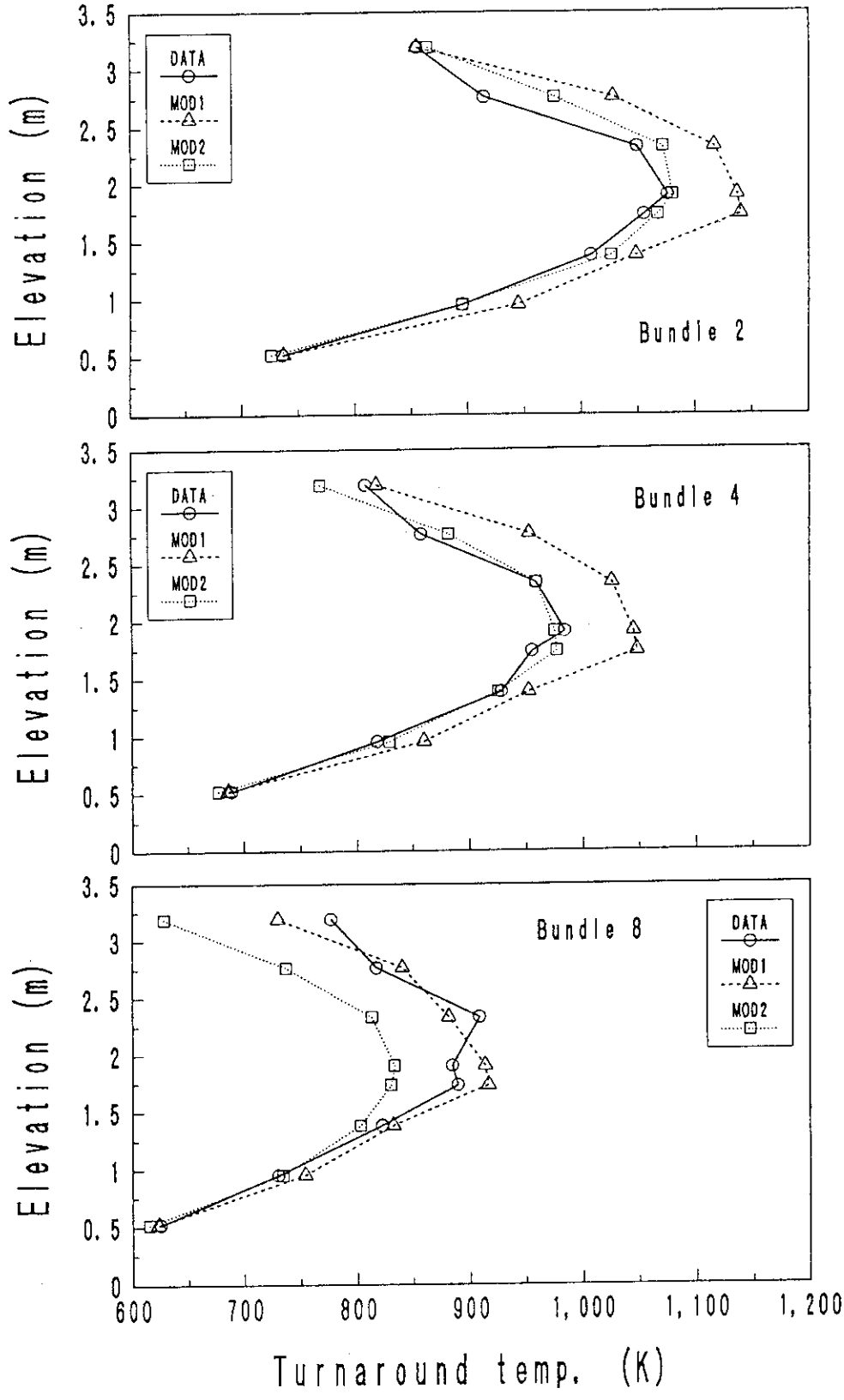

Fig. 4.3.4 Comparison of turnaround temperature in bundles 2, 4 and 8

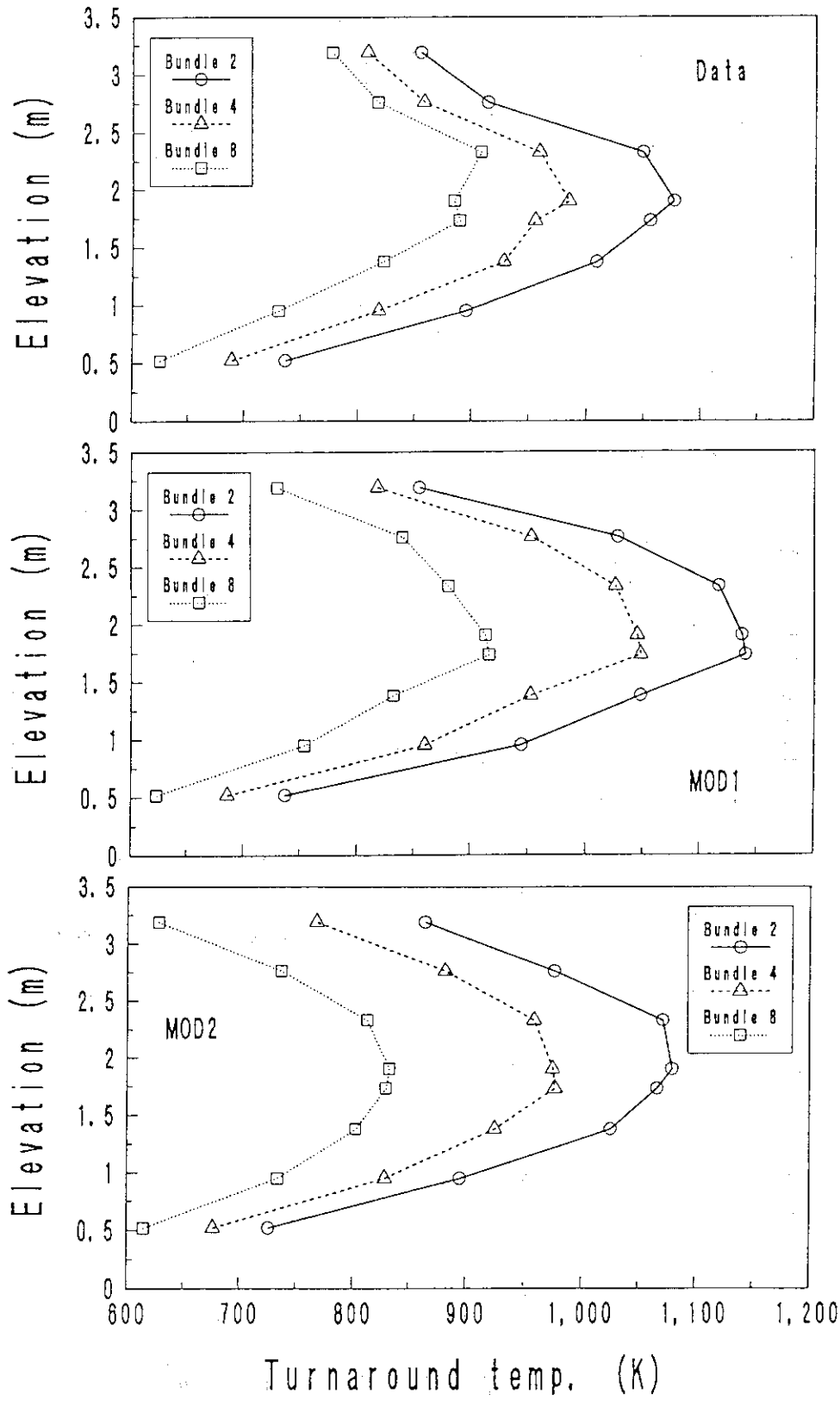

Fig. 4.3.5 Comparison of radial distribution of turnaround temperature

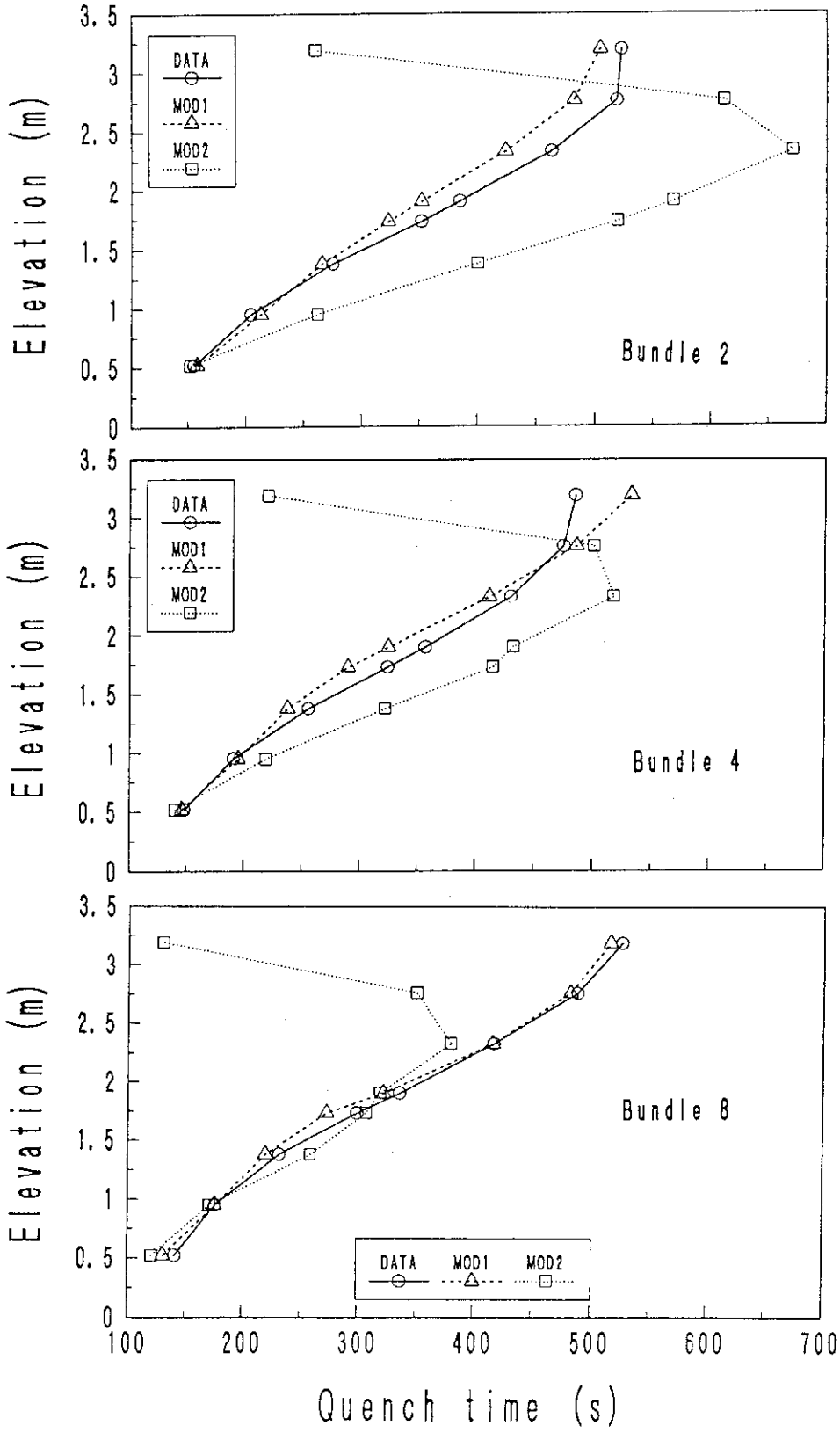

Fig. 4.3.6 Comparison of quench time in bundles 2, 4 and 8

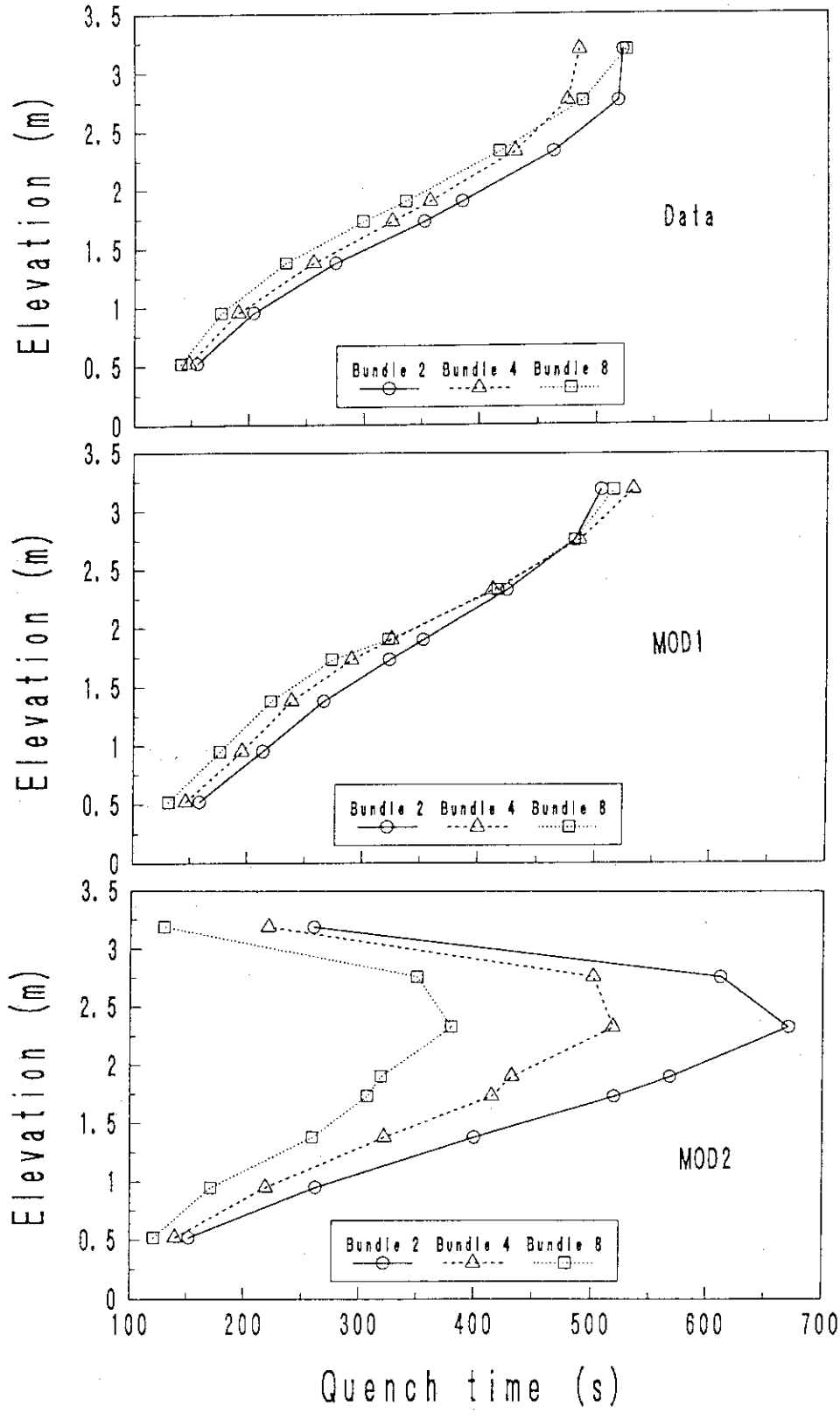

Fig. 4.3.7 Comparison of radial distribution of quench time

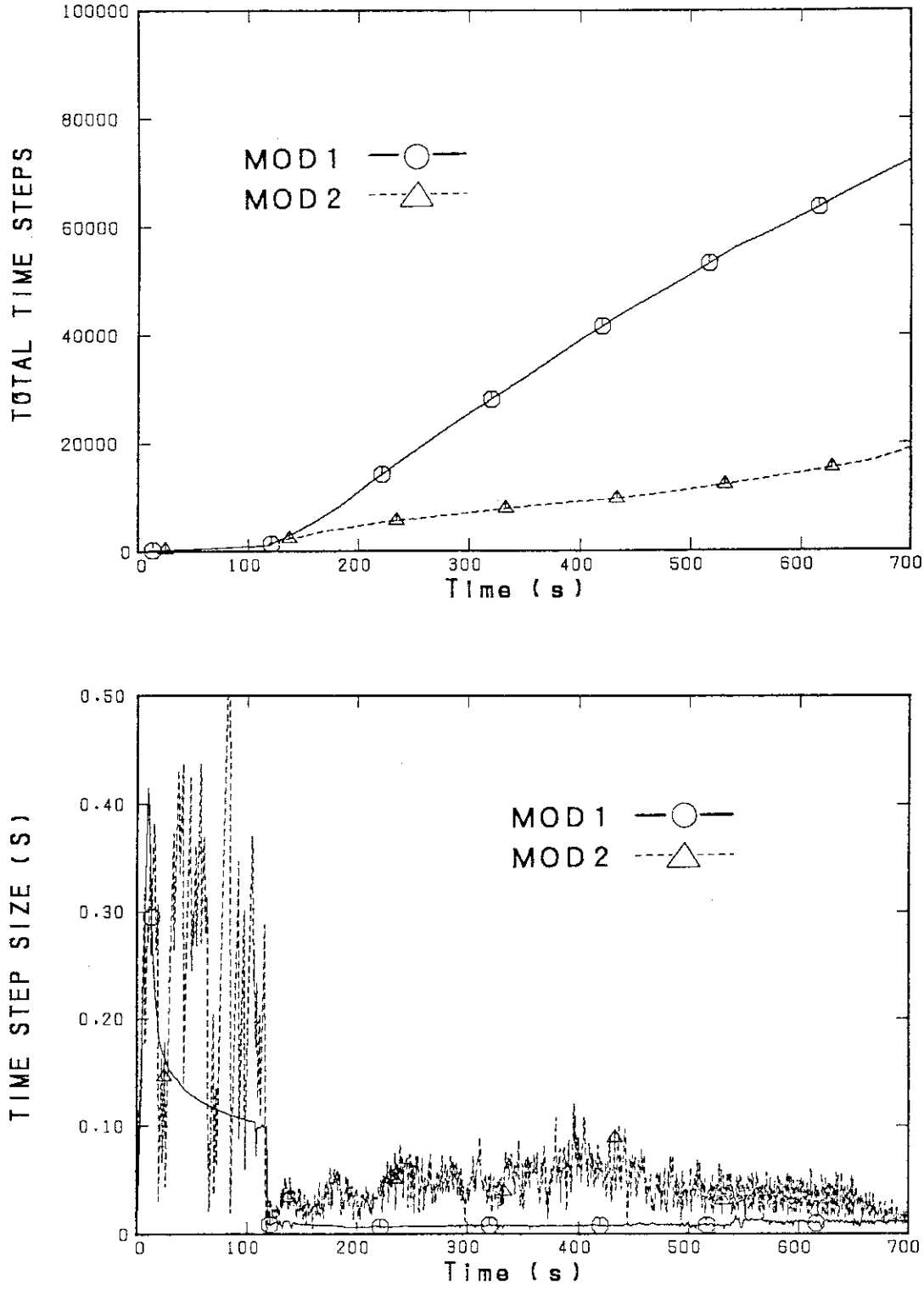

Fig. 4.4.1 Comparison of total time step (upper figure) and time step size (lower figure)